DOI: https://doi.org/10.24297/jac.v16i0.8099

Structural And Vibrational Studies on Isomers of Antiviral Ribavirin Drug in Gas and Aqueous Environmental by Using The SQM Approach

María F. Ladetto[a], María J. Márquez[a], Davide Romani[b], Silvia A. Brandán[a,*]

[a]Cátedra de Química General, Instituto de Química Inorgánica, Facultad de Bioquímica, Química y Farmacia, Universidad Nacional de Tucumán, Ayacucho 4z71,(4000), San Miguel de Tucumán, Tucumán, Argentina.

[b]SST, Servicio sanitario della Toscana, Azienda USL 9 Toscana SudEst di Grosseto, Via Cimabue, 109, 58100 Grosseto, Italia.

sbrandan@fbqf.unt.edu.ar

Abstract

Five stable isomers of antiviral ribavirin agent were theoretically determined in gas and aqueous solution by using the hybrid B3LYP/6-31G* method. Here, the solvent effects were studied with the self consistent reaction field (SCRF) methodology employing the polarized continuum (PCM) and the universal solvation model (SM). Structural, electronic and topological properties were reported for all isomers while the vibrational analyses were performed only for those two polymorphic structures experimentally observed in the solid phase by X-ray diffraction. Calculations have evidenced that C2 correspond to the polymorphic V1 structure while C5 to the polymorphic V2 structure. The high dipole moment values predicted for C2 and C5 in both media could probably explain their presences in the solid. Experimental available IR and Raman spectra of ribavirin in the solid state and normal internal coordinates were employed together with the scaled quantum mechanical force field (SQMFF) approach to perform the complete vibrational assignments in both media. Here, the 81 vibration modes expected for C2 and C5 in both media were completely assigned. The frontier orbitals studies reveal that C5 is the less reactive in both media. Here, the gap value observed for C5 is in agreement with the value recently reported for ribavirin by using B3LYP/6-311++G** calculations.

Keywords: Ribavirin, vibrational spectra, molecular structure, force field, DFT calculations

1. Introduction

Ribavirin or virazole is an antiviral drug whose chemical name is 1-β-D-ribofuranosyl-1,2,4-triazole-3-carboxamide and, as it present activity on various DNA and RNA viruses, in particular orthomyxoviruses (influenza A and B), paramyxoviruses (measles, respiratory syncytial virus (RSV)) and arenaviruses (Lassa, Junin, etc.), as reported by De Clercq [1] their study is of great chemical, pharmacological and medicinal interest. Usually, this drug is used alone for chronic hepatitis C virus infection or in combination with other with similar effects [2-6]. However, the application of ribavirin on various systems is strictly limited by the peak-to-trough fluctuation in plasma drug concentrations and some undesirable side-effects, as suggested by Chen et al. [6]. Besides, the antiviral drugs designed to accelerate viral mutation rates can drive a viral population to extinction in a process called lethal mutagenesis, as mentioned in a recent study by Pen et al. [7]. For these reasons, it is necessary and useful to improve the properties of this interesting drug of wide clinical use in order to diminish their side effects and the adverse reactions. Normally, the biological activity of a substance is closely related with the presence of hydrophobic and hydrophilic regions in its structure, as observed by Urzúa et al. [8] in a study on the antibacterial activities of some terpenoids. Hence, the use of structure-activity relationship (SAR) methods is of importance to the design of new and better drugs [9-13]. On the other hand, the complete assignments of the vibrational spectra of ribavirin in solid and aqueous solution are of great importance because

they allow their quick identification in all the systems by using the vibrational spectroscopy, as observed for other antiviral agents [14-18]. So far, the temperature effects on the FTIR spectra of Ribavirin were recently reported by Topala [19], the IR spectrum at room temperature by Kumar [20] and new studies by Near-Infrared and Raman Spectroscopies [21,22] were recently reported but, in this latter work all isomers were not studied and the complete assignments of their vibrational spectra were not performed by using their force fields. In this context, in order to characterize completely this antiviral substance, in relation to their interesting biological activities, the aims of the present work are the studies of the structural, electronic, topological and vibrational properties of all isomers in gas phase and, especially in aqueous solution, because it is known that ribavirin are soluble in water. For these purposes, the DFT calculations were carried out in order to optimize the molecule by using the hybrid B3LYP/6-31G* method in gas phase [23,24] while, in aqueous solution, the calculations were performed with the PCM and solvation models which consider the solvent effects [25-27]. Here, the volume variations that experiment the species in aqueous solution were calculated with the Moldraw program [28]. Then, their reactivities and behaviors in both media were predicted at the same level of theory by using the frontier orbitals energies [29,30] and the equations reported in the literature for the chemical potential (μ), electronegativity (χ), global hardness (η), global softness (S) and global electrophilicity (ω) and nucleophilicity (ε) indexes descriptors [31-43]. Moreover, the hydrophobic and hydrophilic regions sites of ribavirin in both phases can be clearly predicted by means of the different colorations observed on the molecular electrostatic potential surfaces mapped. In addition, the force fields and the force constants were also calculated in both media by using the SQMFF methodology and the Molvib program [44,45]. Here, we have compared the properties of ribavirin in the two studied media with those computed properties by us for other antiviral drugs such as, thymidine [14,18], dideoxynucleoside zalcitabine [46], 5-trifluoromethyluracil [47] and cidofovir and brincidofovir [48] in order to observe the relationships that exist between the hydrophobic and hydrophilic sites and the different groups because it is very important to understand the mechanisms of interaction of this antiviral agent with the receptors sites.

2. Materials and Methods

Computational details

Here, five different stable structures of ribavirin were proposed due to the presence of two chiral C atoms in the sugar ring, as reported for emtricitabine by Sanmarti et al. [17,49]. Thus, three *Cis* isomers and two *Trans* isomers of ribavirin were studied in order to know which of them are the two structures experimentally observed by X-ray diffraction by Prusiner and Sundaralingam [50]. The initial structures were modelled with the *GaussView* program [51] and, then optimized in gas phase by using the hybrid B3LYP/6-31G* level of theory [23,24] with the Gaussian 09 program [52] while the solvent effects in aqueous solution were considered by using the SCRF method together with the PCM and solvation models (SM) [25-27]. Hence, the solvation energies were easily computed with the universal SM model at the same calculation level. The five structures, named C1, C2, C3, C4 and C5 are given in **Figure 1** together with the atoms labelling. Here, the NBO [53,54] and AIM [55,56] calculations at the same level of theory were employed to calculate the natural population atomic (NPA), the bond orders, the stabilization energies and the topological analysis of the electronic charge densities. Additionally, the charges derived from Merz-Kollman [57] were also calculated while the electrostatic potential surfaces mapped were generated with the *GaussView* program [50]. The harmonic force fields for those five isomers were calculated in Cartesian coordinates at the same level of theory employing the SQMFF methodology [44] and the Molvib program [45]. Then, the transformations to natural internal coordinates were carrying out using that latter program. Here, the definition of the natural internal coordinates were not presented for ribavirin because they are similar to those reported for compounds with analogous rings and groups [14-18,31-42,46-48].

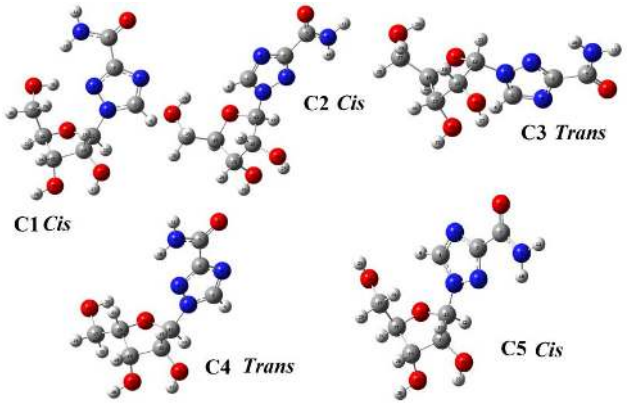

Figure 1. Theoretical molecular structures of most stable isomers of ribabirin and the atoms labelling.

The tentative assignments of the most stable configurations were performed taking into account the potential energy distributions (PED) ≥ 10 % and, in some cases, values lower than 10% were considered due to coupling of modes. The reactivities and behaviours of all isomers of ribavirin in the two studied media were predicted by using the calculated frontier orbitals and the μ, χ, η, S, ω and ε descriptors at B3LYP/6-31G* level of theory [29,30]. Here, the obtained properties for ribavirin were compared with the values reported for thymidine [14], dideoxynucleoside zalcitabine [46], 5-trifluoromethyluracil [47] and cidofovir and brincidofovir [48]. The knowledge of the nucleophilic or electrophilic sites is clearly important to find those reacting regions with the potential biological agents due to their antiviral activities.

3. Results and Discussion

3.1 Geometries, volume, solvation energies

The calculated total and relative energies, dipole moments and populations for the five isomers of ribavirin in both media using the B3LYP/6-31G* method can be seen in **Table 1** while their differences in function of the different structures are represented in **Figures 2**.

Table 1. Total (*E*) and relative (ΔE) energies, dipole moment (μ) and populations for all the isomers of ribavirin in both media by using the B3LYP/6-31G* method

Gas phase				
Isomer	E (Hartrees)	ΔE (kJ/mol)	μ (D)	Population
C1 (*Cis*)	-907.1549	0.00	8.43	88.59
C2(*Cis*)	-907.1493	14.69	8.67	0.23
C3(*Trans*)	-907.1506	11.28	7.30	0.88
C4(*Trans*)	-907.1525	5.33	8.24	10.28
C5(*Cis*)	-907.1465	22.03	8.84	0.02
Aqueous solution				
Isomer	E (Hartrees)	ΔE (kJ/mol)	μ (D)	Population
C1 (*Cis*)	-907.2027	0.00	11.60	38.17
C2(*Cis*)	-907.2015	3.15	11.63	10.69
C3(*Trans*)	-907.2015	3.15	10.59	10.69
C4(*Trans*)	-907.2027	0.00	11.76	38.17
C5(*Cis*)	-907.2000	7.08	12.55	2.28

On the other hand, the volume variations that experiment those five isomers in solution and their solvation energy values are summarized in **Table 2** while **Figure 3** shows their behaviours in both media. Thus, regarding the energy values of Figure 2 we observed that the C1 and C4 isomers are the most stable isomers in both media while C5 is the most unstable isomer in those media because this isomer has high energies barriers, especially in gas phase. The dipole moments of the five isomers show a similar behaviour in both media where clearly it is observed that C3 present the lowest values while C5 the higher ones. Note that all the values in solution are higher than those in gas phase, as expected because the isomers are hydrated in solution due to the H bonds formation with the water molecules. In relation to the populations in both media, the C1 and C4 isomers have the higher populations while C2, C3 and C5 the most low, as observed in Figure 2. On the other hand, analyzing the molar volumes according to Figure 3 the same behaviours are expected for C4 and C5 in both media while from C1 to C3 we observed an increase in the corresponding values.

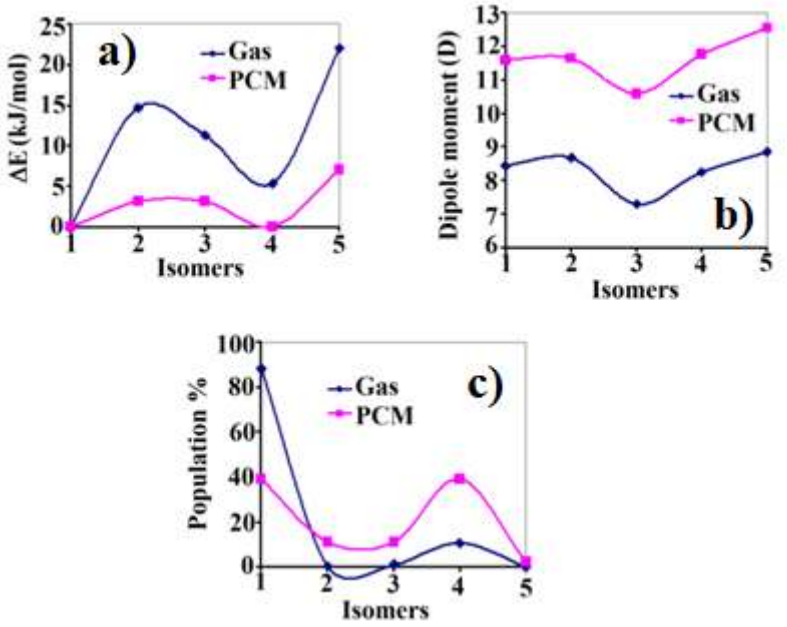

Figure 2. Variations observed in the relative energies (a), dipole moment values (b) and populations % (c) for the five isomeric structures of ribavirin in gas and aqueous solution phases at B3LYP/6-31G* level of theory.

Table 2. Molecular volume for the stable configurations of ribavirin by using the B3LYP/6-31G* method

Ribavirin			
Isomer	Molar Volume (Å^3)		$^{\#}\Delta V = V_{AS} - V_G$ (Å^3)
	GAS	PCM/SMD	
C1	216.9	221.2	4.3
C2	223.9	226.2	2.3
C3	224.4	226.7	2.3
C4	224.8	225.4	0.6
C5	234.6	233.5	-1.1
ΔG (kJ/mol)			
Isomer	$\Delta G_u^{\#}$	ΔG_{ne}	ΔG_c
C1	-125.38	16.47	-141.85
C2	-136.92	13.92	-150.84
C3	-133.51	15.63	-149.14
C4	-131.67	16.72	-148.39
C5	-140.33	15.84	-156.17

$$\Delta G_c = \Delta G_{uncorrected}^{\#} - \Delta G_{Total\ non\text{-}electrostatic}$$

This way, Table 2 shows clearly volume expansion for all the isomers in solution, with exception of C5 where it is observed a volume contraction. It is very important to observe that the non electrostatic terms, calculated by using the SM model, are positive in all the isomers, hence, the corrected solvation energies present the more negative values, in reference to the uncorrected ones, as can be seen in Figure 3. Probably, the higher volume variation observed for C1 in solution is justified by the higher increase of their dipole moment value. Here, the high solvation energy value for C2 (most negative value) could maybe justify in part their presence in solution while the lower value in C1 are attributed to the higher non-electrostatic terms and to their lower volume values in both media.

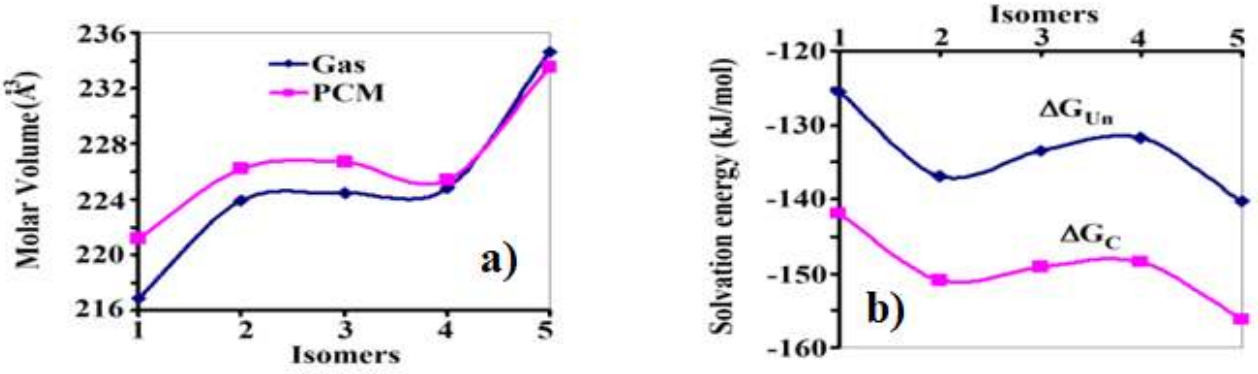

Figure 3. Variations observed in the molar volume (a) and in the solvation energy values (b) for the five isomeric structures of ribavirin in aqueous solution phase at B3LYP/6-31G* level of theory.

The calculated geometrical parameters for the five structures of ribavirin in gas phase can be seen in **Table 3** compared with the experimental V1 and V2 structures reported by Prusiner and Sundaralingam [50] by means of the root-mean-square deviation (RMSD) values. First, we observed that the bond lengths are similar for all isomers independently of their *Cis* or *Trans* structures and, besides these parameters present the better correlations when they are compared with V1 (0.018-0.020 Å) than when are compared with V2 (0.020-0.021 Å). These correlations can be graphically seen in **Figures 4** and **5**. Figure 5 show clearly the higher observed differences in the C7-N9, C1-N3, C1-N6 and N3-N5 bond lengths. On the contrary, analyzing the bond angles values it is observed a better correlation of the calculated parameters using the same calculation level with the V2 structure (1.2-1.4º) than with V1 (1.2-3.0º). The higher variations are observed in the dihedral angles related to the two triazole and ribofuran rings present in ribavirin showing variations from 262.8 up to 12.2º. However, the better correlations observed in the dihedral angles show that the conformations C2 and C5 correspond to those two polymorphic crystalline forms V1 and V2 reported by Prusiner and Sundaralingam [50] where the conformation about the exocyclic C16-C15 bond is *gauche* in C2 and *trans* in C5, as in those experimental V1 and V2 structures [50], then, these two forms are those two experimentally observed, as observed in **Figure 6**. Here, the volume expansion and contraction for C2 and C5 together with their higher dipole moment values in solution, respectively could clearly justify their higher solvation energies (Table 2) and the high solubility in water observed for ribavirin.

Table 3. Comparison of calculated geometrical parameters for the stable isomers in gas phase with the corresponding experimental ones

Parameter	B3LYP/6-31G* Method[a]					Experimental[b]	
	C1	C2	C3	C4	C5	V2	V1
	Bond lengths (Å)						
C1-N3	1.356	1.360	1.359	1.358	1.358	1.340	1.327

C1-N6	1.321	1.316	1.318	1.316	1.321	1.321	1.332
N3-N5	1.350	1.354	1.353	1.353	1.349	1.359	1.368
N3-C12	1.469	1.447	1.461	1.456	1.472	1.484	1.475
N5-C2	1.332	1.330	1.330	1.331	1.334	1.307	1.321
C2-C7	1.502	1.501	1.500	1.501	1.499	1.491	1.487
N6-C2	1.361	1.366	1.364	1.364	1.361	1.362	1.361
C7-O8	1.220	1.220	1.220	1.219	1.220	1.232	1.235
C7-N9	1.366	1.365	1.366	1.366	1.366	1.322	1.328
C12-O14	1.404	1.422	1.411	1.413	1.405	1.409	1.393
C12-C13	1.561	1.548	1.563	1.557	1.562	1.530	1.528
C13-O23	1.401	1.397	1.394	1.401	1.399	1.418	1.427
C13-C15	1.546	1.540	1.544	1.541	1.551	1.537	1.523
C15-O25	1.426	1.428	1.428	1.431	1.425	1.415	1.418
C15-C16	1.530	1.538	1.530	1.530	1.533	1.537	1.519
C16-O14	1.446	1.450	1.454	1.445	1.438	1.454	1.464
C16-C17	1.545	1.528	1.530	1.522	1.529	1.502	1.509
C17-O18	1.410	1.411	1.411	1.415	1.417	1.424	1.435
$RMSD_{V1}$	**0.020**	**0.019**	**0.019**	**0.018**	**0.019**		
$RMSD_{V2}$	**0.021**	**0.021**	**0.021**	**0.020**	**0.021**		
Bond angles (°)							
O8-C7-N9	124.1	124.1	124.0	124.1	123.9	123.2	123.8
C2-C7-N9	113.8	113.5	113.5	113.6	113.3	115.9	116.7
C2-C7-O8	122.1	122.4	122.5	122.4	122.5	120.1	119.4
N6-C2-C7	124.2	123.3	123.4	123.1	123.6	121.2	122.1
N5-C2-C7	121.5	122.0	121.9	122.1	121.6	123.4	122.3
N6-C2-N5	114.3	114.7	114.7	114.7	114.7	115.4	115.5
C1-N6-C2	102.7	102.7	102.8	102.6	102.8	102.1	102.1
N3-C1-N6	110.7	110.7	110.5	110.8	110.1	110.6	110.5
C1-N3-N5	109.0	109.1	109.3	109.1	109.7	109.3	110.3
N3-N5-C2	103.2	102.8	102.7	102.7	102.5	102.5	101.6
N5-N3-C12	120.2	120.9	119.6	121.7	120.7	117.6	118.9
C1-N3-C12	130.8	130.0	131.1	129.0	129.5	133.0	130.8
O14-C12-C13	110.6	104.9	106.2	107.3	108.1	106.2	107.7
C16-O14-C12	110.6	110.1	111.9	110.3	110.2	110.0	109.7
C15-C16-O14	104.4	106.5	106.2	104.7	104.4	106.1	104.0
C16-C15-C13	102.3	103.2	103.0	101.9	103.0	103.6	101.6
C15-C13-C12	102.2	101.0	103.0	102.4	102.3	101.1	101.3
O14-C12-N3	109.0	108.9	110.4	110.6	108.3	109.0	107.9
N3-C12-C13	112.9	115.0	114.0	112.6	112.1	112.8	111.4
C12-C13-O23	113.8	114.9	115.8	114.0	114.4	104.4	106.0
C15-C13-O23	114.0	114.5	114.5	114.0	113.2	112.1	111.6
C13-C15-O25	105.0	104.8	105.8	105.5	105.3	113.9	109.7
C16-C15-O25	113.0	112.7	112.7	113.2	111.7	114.6	113.6
C17-C16-C15	112.7	114.9	114.8	117.3	113.2	111.8	117.7
C17-C16-O14	111.2	107.2	107.7	106.8	112.3	110.3	108.3
C16-C17-O18	112.0	111.2	11.0	111.3	107.6	111.4	110.2
$RMSD_{V1}$	**3.0**	**1.3**	**1.2**	**1.5**	**1.4**		
$RMSD_{V2}$	**1.2**	**1.3**	**1.4**	**1.3**	**1.2**		
Dihedral angle (º)							

C16-O14-C12-	7.0	-26.1	-8.2	4.7	13.1	25.2	4.6
O14-C12-C13-	15.7	37.1	24.5	18.1	9.2	-35.7	-27.1
C12-C13-C15-C16	-30.8	-33.8	-30.6	-32.3	-26.1	32.3	37.8
C13-C15-C16-	35.9	19.9	26.6	36.2	34.6	-18.9	-36.1
C15-C16-O14-	-27.4	3.9	-11.8	-26.1	-30.3	-3.8	20.1
$RMSD_{V1}$	**45.9**	**52.7**	**46.5**	**46.9**	**42.7**		
$RMSD_{V2}$	**52.9**	**52.1**	**49.9**	**53.5**	**51.0**		
			Glycosyl torsion angle, χ (°)				
O14-C12-N3-$C1_G$	-142.9	58.0	-41.2	-107.5	-2.6	10.4	119.0
O14-C12-N3-$C1_S$	-144.6	57.4	-35.6	-107.7	21.7	10.4	119.0
$RMSD_{V1}$	**154.2**	**47.3**	**48.9**	**118.0**	**12.2**		
$RMSD_{V2}$	**262.8**	**61.3**	**157.4**	**226.6**	**110.1**		

[a]This work, [b]From Ref [50]

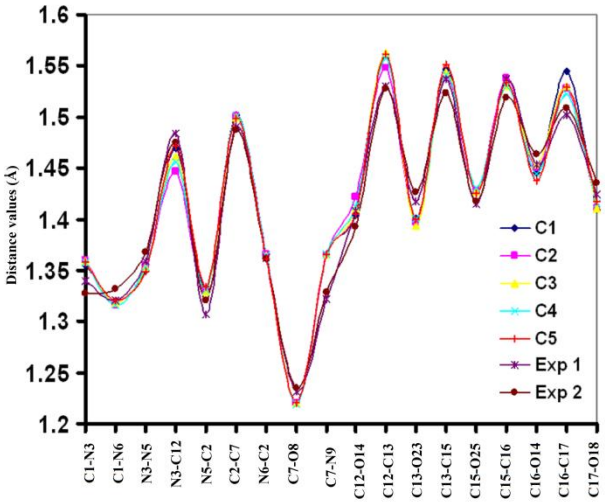

Figure 4. Variations observed in the bond lengths for the four isomeric structures of ribavirin in gas phase at B3LYP/6-31G* level of theory and their comparison with the corresponding experimental ones.

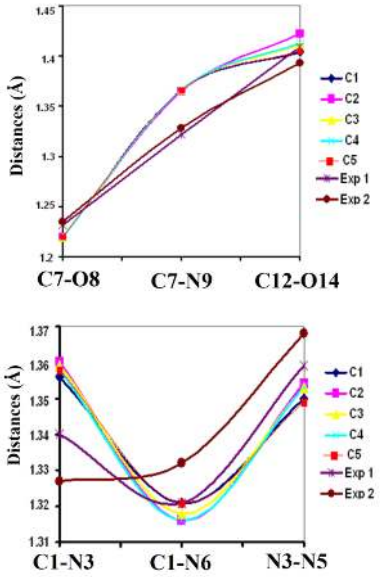

Figure 5. Variations observed in the bond lengths for the four isomeric structures of ribavirin in gas phase at B3LYP/6-31G* level of theory and their comparison with the corresponding experimental ones.

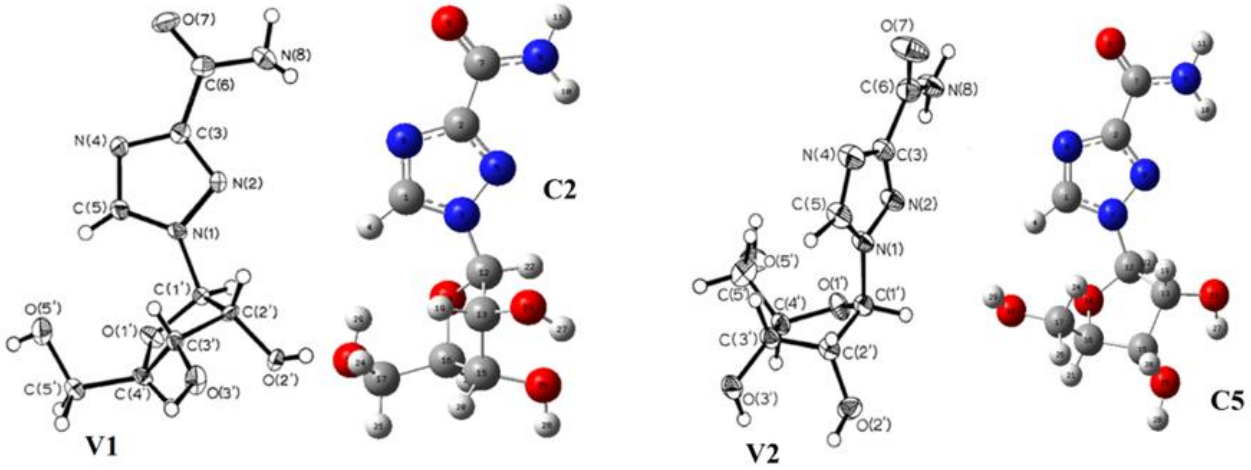

Figure 6. Molecular structures of C2 and C5 isomers compared with the corresponding to those two experimental polymorphic crystalline forms V1 and V2.

Moreover, the populations of C2 and C5 increase slightly in solution probably due to the higher solubility in this medium. Obviously, the differences observed between the gas phase and the solid state can easily attributed to the calculations because the packing forces in solid phase were not considered in the calculations in gas phase while the H bonds forces are important in solution. Another very important result is that the optimized structures for the two conformers predicted higher double C=O bonds character of the amide form in the gas phase than in aqueous solution, as shown in Table 3. Analyzing the distances values between the more electronegative atoms for the stable conformations of ribavirin presented in **Table 4** we observed that a possible justification of the low population of C2 in gas phase can be attributed to the proximities between the more electronegative atoms.

Table 4. Comparison of calculated geometrical parameters for the stable isomers of ribavirin in gas phase and in aqueous solution by using the B3LYP/6-31G* method.

Isomer	Gas			Aqueous solution		
	N6---O8	N3---O14	N14---O18	N6---O8	N3---O14	N14---O18
C2	2.904	2.334	2.766	2.865	2.348	2.793
C5	2.913	2.332	2.821	2.864	2.335	2.811

Thus, in that conformer the N6---O8, N3---O14 and N14---O18 distances in gas phase are slight lower in C2 than C5 while in solution the distance between these atoms are practically the same in the two conformers, as observed in Table 4.

3.2. Atomic charges, electrostatic potentials, bond orders

The atomic charges were studied for all isomers of ribavirin in gas and aqueous solution phases by using the B3LYP/6-31G* method. The natural (NPA) and MK charges [57] observed on all the atoms of all isomers in both media are presented in **Tables 5** and **6**. Here, the behaviours of both charges on the N and O atoms involved principally in the nucleophilic and electrophilic sites of ribavirin in both media were exhaustively analyzed. In

general, we observed that both charges have different values and that the NPA charges have higher values than the other ones in both conformers and show few variations in the different media.

Table 4. Atomic MK and NPA charges for all isomers of Ribavirin in gas phase

Atoms	MK					NPA				
	C1	C2	C3	C4	C5	C1	C2	C3	C4	C5
C 1	0.365	0.268	0.296	0.319	0.341	0.205	0.200	0.202	0.208	0.189
C 2	0.451	0.632	0.588	0.506	0.525	0.269	0.251	0.249	0.258	0.247
N 3	-0.086	0.196	0.151	0.038	0.150	-0.219	-0.221	-0.233	-0.223	-0.231
H 4	0.079	0.105	0.114	0.091	0.075	0.239	0.232	0.242	0.235	0.253
N 5	-0.318	-0.598	-0.596	-0.449	-0.552	-0.355	-0.302	-0.309	-0.325	-0.321
N 6	-0.604	-0.643	-0.650	-0.605	-0.649	-0.463	-0.460	-0.468	-0.464	-0.474
C 7	0.557	0.481	0.505	0.552	0.542	0.642	0.644	0.644	0.644	0.643
O 8	-0.483	-0.475	-0.482	-0.487	-0.489	-0.585	-0.588	-0.590	-0.585	-0.592
N 9	-0.893	-0.840	-0.836	-0.876	-0.873	-0.852	-0.851	-0.852	-0.852	-0.853
H 10	0.356	0.364	0.363	0.360	0.377	0.421	0.423	0.422	0.420	0.424
H 11	0.422	0.408	0.402	0.417	0.408	0.420	0.419	0.417	0.419	0.417
C 12	0.147	0.101	0.268	-0.004	0.041	0.247	0.248	0.250	0.246	0.254
C 13	0.283	0.187	0.204	0.446	0.388	0.056	0.061	0.055	0.057	0.056
O 14	-0.305	-0.347	-0.433	-0.295	-0.390	-0.574	-0.605	-0.596	-0.598	-0.572
C 15	0.056	0.113	0.113	-0.153	-0.098	0.042	0.041	0.037	0.043	0.045
C 16	-0.045	-0.046	-0.109	0.175	0.266	0.028	0.027	0.024	0.026	0.035
C 17	0.251	0.119	0.307	0.176	0.014	-0.123	-0.111	-0.114	-0.113	-0.124
O 18	-0.569	-0.539	-0.607	-0.575	-0.570	-0.762	-0.742	-0.743	-0.744	-0.748
H 19	0.093	0.067	0.077	0.044	0.049	0.248	0.237	0.245	0.257	0.247
H 20	0.052	0.053	0.050	0.100	0.079	0.232	0.232	0.235	0.235	0.229
H 21	0.125	0.127	0.140	0.022	0.090	0.246	0.241	0.247	0.238	0.252
H 22	0.099	0.150	0.087	0.109	0.144	0.247	0.252	0.256	0.244	0.254
O 23	-0.640	-0.581	-0.589	-0.637	-0.632	-0.744	-0.737	-0.733	-0.743	-0.740
H 24	-0.056	0.013	-0.038	0.060	0.028	0.196	0.190	0.192	0.220	0.202
O 25	-0.602	-0.612	-0.660	-0.536	-0.580	-0.772	-0.774	-0.776	-0.777	-0.769
H 26	0.044	0.081	0.036	0.008	0.040	0.225	0.224	0.225	0.206	0.205
H 27	0.436	0.415	0.426	0.409	0.424	0.494	0.493	0.495	0.490	0.493
H 28	0.432	0.429	0.456	0.409	0.426	0.495	0.495	0.497	0.496	0.494
H 29	0.352	0.371	0.413	0.378	0.423	0.496	0.483	0.483	0.482	0.485

Table 5. Atomic MK and NPA charges for all isomers of Ribavirin in aqueous solution

Atoms	MK					NPA				
	C1	C2	C3	C4	C5	C1	C2	C3	C4	C5
C 1	0.362	0.244	0.417	0.281	0.299	0.204	0.189	0.201	0.206	0.188
C 2	0.475	0.650	0.385	0.522	0.619	0.268	0.251	0.248	0.258	0.247
N 3	-0.074	0.166	-	0.120	0.133	-0.217	-0.221	-	-	-0.224
H 4	0.077	0.119	-	0.098	0.091	0.239	0.227	0.240	0.234	0.244
N 5	-0.355	-0.609	-	-	-0.590	-0.352	-0.300	-	-	-0.312
N 6	-0.604	-0.643	0.581	-	-0.657	-0.459	-0.456	-	-	-0.468
C 7	0.539	0.464	-	0.535	0.493	0.632	0.634	0.634	0.634	0.634
O 8	-0.489	-0.481	-	-	-0.494	-0.593	-0.597	-	-	-0.602

N 9	-0.868	-0.823	0.432	-	-0.839	-0.839	-0.839	-	-	-0.841
H 10	0.353	0.366	0.276	0.357	0.369	0.418	0.422	0.422	0.420	0.423
H 11	0.422	0.407	-	0.412	0.407	0.424	0.422	0.420	0.422	0.419
C 12	0.186	0.255	0.186	-	0.118	0.247	0.245	0.255	0.248	0.255
C 13	0.219	0.117	0.281	0.383	0.296	0.051	0.055	0.051	0.054	0.054
O 14	-0.319	-0.366	0.240	-	-0.404	-0.572	-0.594	-	-	-0.573
C 15	0.080	0.144	-	-	-0.095	0.041	0.041	0.035	0.043	0.044
C 16	-0.024	-0.077	-	0.201	0.258	0.030	0.027	0.025	0.027	0.036
C 17	0.227	0.146	-	0.139	0.126	-0.125	-0.119	-	-	-0.123
O 18	-0.572	-0.544	0.417	-	-0.599	-0.760	-0.742	-	-	-0.745
H 19	0.112	0.071	0.385	0.065	0.069	0.249	0.241	0.243	0.259	0.245
H 20	0.048	0.049	-	0.088	0.086	0.232	0.233	0.234	0.235	0.230
H 21	0.125	0.141	-	0.027	0.086	0.250	0.249	0.249	0.240	0.252
H 22	0.093	0.109	-	0.122	0.140	0.245	0.257	0.254	0.239	0.251
O 23	-0.631	-0.570	0.581	-	-0.596	-0.745	-0.738	-	-	-0.738
H 24	-0.050	-0.010	-	0.067	-0.011	0.195	0.187	0.196	0.219	0.200
O 25	-0.590	-0.594	-	-	-0.575	-0.770	-0.770	-	-	-0.767
H 26	0.049	0.079	0.432	0.022	0.010	0.225	0.229	0.226	0.210	0.206
H 27	0.426	0.405	0.276	0.399	0.410	0.491	0.492	0.496	0.487	0.490
H 28	0.423	0.419	-	0.397	0.425	0.495	0.494	0.498	0.495	0.493
H 29	0.359	0.368	0.186	0.387	0.425	0.494	0.482	0.482	0.481	0.482

In relation to the N atoms, it is observed that the MK charge on the N5 atoms in C1 is different from the corresponding to C2 in gas phase and, the value in C2 decreases notably in solution. On the other hand, the MK charges on the N9 atoms of all isomers in both media present the higher values, as expected because those atoms belong to the NH_2 groups. In both media, the behaviours of these charges on the N6 atoms of all isomers are practically similar among them. Analyzing the O atoms, both charges show higher values on the O18 and O23 atoms of all isomers evidencing the following tendency: O23 > O18 > O8 > O14 in both media although the values little change in solution.

The molecular electrostatic potentials (MEP) were also studied for all isomers in both media because they are of interest to investigate the different sites of reactivity of ribavirin taking into account that when it is used as an antiviral drug interaction with different nucleophiles or electrophiles reactive. Thus, **Table 6** shows the MEP values on all the atoms of all isomers of ribavirin in both media.

Table 6. Molecular electrostatic potential (in a.u.) for five isomersof ribavirin in both media.

Atoms	Gas phase					Aqueous solution				
	C1	C2	C3	C4	C5	C1	C2	C3	C4	C5
C 1	-	-	-	-	-14.676	-14.656	-14.659	-14.672	-14.662	-14.677
C 2	-	-	-	-	-14.689	-14.673	-14.681	-14.689	-14.681	-14.692
N 3	-	-	-	-	-18.256	-18.240	-18.244	-18.254	-18.247	-18.257
H 4	-1.049	-1.052	-1.065	-1.053	-1.073	-1.049	-1.049	-1.067	-1.054	-1.072
N 5	-	-	-	-	-18.331	-18.311	-18.321	-18.330	-18.322	-18.333
N 6	-	-	-	-	-18.371	-18.356	-18.360	-18.370	-18.363	-18.374
C 7	-	-	-	-	-14.644	-14.634	-14.639	-14.645	-14.639	-14.647
O 8	-	-	-	-	-22.368	-22.362	-22.367	-22.372	-22.367	-22.375
N 9	-	-	-	-	-18.335	-18.321	-18.325	-18.330	-18.324	-18.332
H 10	-1.013	-1.015	-1.018	-1.012	-1.021	-1.007	-1.012	-1.017	-1.010	-1.019
H 11	-1.017	-1.017	-1.020	-1.015	-1.023	-1.010	-1.013	-1.018	-1.012	-1.020

C 12	-	-	-	-	-14.626	-14.615	-14.618	-14.617	-14.618	-14.626
C 13	-	-	-	-	-14.659	-14.653	-14.649	-14.650	-14.658	-14.657
O 14	-	-	-	-	-22.278	-22.279	-22.274	-22.267	-22.283	-22.281
C 15	-	-	-	-	-14.648	-14.648	-14.644	-14.642	-14.650	-14.647
C 16	-	-	-	-	-14.658	-14.665	-14.657	-14.656	-14.664	-14.657
C 17	-	-	-	-	-14.660	-14.676	-14.664	-14.663	-14.671	-14.658
O 18	-	-	-	-	-22.287	-22.316	-22.300	-22.298	-22.304	-22.288
H 19	-1.083	-1.078	-1.080	-1.089	-1.091	-1.081	-1.075	-1.079	-1.086	-1.084
H 20	-1.075	-1.072	-1.069	-1.074	-1.075	-1.071	-1.069	-1.066	-1.074	-1.072
H 21	-1.088	-1.087	-1.082	-1.094	-1.085	-1.091	-1.084	-1.082	-1.093	-1.084
H 22	-1.072	-1.080	-1.078	-1.074	-1.088	-1.072	-1.080	-1.078	-1.075	-1.089
O 23	-	-	-	-	-22.300	-22.291	-22.290	-22.293	-22.294	-22.297
H 24	-1.108	-1.098	-1.097	-1.095	-1.089	-1.105	-1.091	-1.092	-1.092	-1.086
O 25	-	-	-	-	-22.267	-22.265	-22.263	-22.259	-22.264	-22.266
H 26	-1.099	-1.091	-1.090	-1.107	-1.088	-1.099	-1.087	-1.087	-1.103	-1.085
H 27	-0.975	-0.974	-0.974	-0.979	-0.983	-0.975	-0.974	-0.977	-0.978	-0.981
H 28	-0.946	-0.944	-0.942	-0.946	-0.948	-0.946	-0.944	-0.940	-0.945	-0.947
H 29	-1.000	-0.986	-0.985	-0.990	-0.970	-1.003	-0.985	-0.983	-0.989	-0.970

The negative MEP values are obviously observed on the O atoms while the less negative values are observed on the H atoms, then the values decrease according to the following order: O > N> C > H. Thus, the more negative values are observed on the N6 and O8 atoms of the two conformers in both media because these two sites are nucleophilic sites while the less negative values are observed on the H28, H27, H10 and H11 atoms due to that these sites are electrophilic sites. This way, on the N6 and O8 atoms are expected strong red colorations in the MEP surface mapped related with the nucleophilic sites acceptors of H bonds. On the other hand, the possible electrophilic sites are those donor of H bonds in the two conformers of ribavirin are those related to the NH_2 and O-H groups and, as a consequence of their lower MEP values strong blue colorations are expected on their corresponding surfaces mapped.

The bond order is a property interesting to investigate the different character and nature of the bonds. Thus, the bond orders expressed as Wiberg indexes for all isomers of ribavirin in both media by using the B3LYP/6-31G* method are presented in **Table 7**.

Table 7. Wiberg indexes for all isomers of Ribavirin in both media

	Gas					Aqueous solution				
Atoms	C1	C2	C3	C4	C5	C1	C2	C3	C4	C5
C 1	3.877	3.884	3.877	3.880	3.869	3.877	3.890	3.880	3.881	3.875
C 2	3.978	3.983	3.984	3.983	3.984	3.981	3.984	3.986	3.985	3.986
N 3	3.571	3.568	3.566	3.568	3.567	3.574	3.573	3.571	3.571	3.573
H 4	0.943	0.947	0.944	0.945	0.940	0.943	0.950	0.944	0.946	0.945
N 5	3.026	3.016	3.015	3.015	3.013	3.026	3.017	3.015	3.016	3.013
N 6	3.060	3.060	3.057	3.060	3.056	3.058	3.059	3.055	3.058	3.055
C 7	3.910	3.908	3.908	3.908	3.908	3.914	3.913	3.912	3.912	3.912
O 8	2.021	2.019	2.017	2.022	2.014	2.002	1.997	1.994	1.999	1.993
N 9	3.030	3.029	3.026	3.027	3.026	3.047	3.045	3.043	3.044	3.043
H 10	0.827	0.823	0.824	0.826	0.822	0.829	0.824	0.824	0.825	0.823
H 11	0.826	0.827	0.829	0.827	0.829	0.823	0.825	0.827	0.825	0.827
C 12	3.816	3.804	3.805	3.818	3.804	3.820	3.807	3.805	3.823	3.808
C 13	3.877	3.887	3.885	3.873	3.880	3.877	3.885	3.887	3.874	3.882

O 14	2.023	1.985	2.004	1.998	2.020	2.020	1.998	2.004	1.995	2.014
C 15	3.855	3.854	3.855	3.853	3.856	3.857	3.858	3.858	3.855	3.858
C 16	3.849	3.850	3.848	3.849	3.856	3.848	3.850	3.848	3.851	3.856
C 17	3.832	3.832	3.831	3.826	3.822	3.834	3.834	3.831	3.827	3.825
O 18	1.789	1.799	1.799	1.794	1.794	1.782	1.795	1.794	1.788	1.792
H 19	0.941	0.946	0.942	0.936	0.942	0.940	0.944	0.943	0.935	0.942
H 20	0.949	0.948	0.947	0.948	0.950	0.948	0.948	0.948	0.948	0.950
H 21	0.943	0.947	0.943	0.949	0.9400	0.941	0.941	0.942	0.947	0.940
H 22	0.942	0.941	0.938	0.943	0.939	0.943	0.938	0.939	0.946	0.941
O 23	1.811	1.820	1.826	1.812	1.815	1.807	1.812	1.816	1.809	1.814
H 24	0.965	0.968	0.967	0.954	0.962	0.965	0.969	0.965	0.954	0.963
O 25	1.788	1.784	1.783	1.788	1.791	1.790	1.787	1.790	1.786	1.790
H 26	0.951	0.952	0.952	0.962	0.961	0.951	0.950	0.951	0.960	0.960
H 27	0.759	0.760	0.757	0.763	0.760	0.762	0.761	0.757	0.766	0.762
H 28	0.756	0.757	0.754	0.755	0.757	0.756	0.757	0.754	0.756	0.758
H 29	0.756	0.769	0.770	0.770	0.766	0.759	0.770	0.770	0.770	0.769

The results show clearly that the O14 atoms in the two media have the higher double bond character, as expected because those atoms belong to the ribofuranosyl rings while the O18 and O25 atoms linked to the H28 and H29 atoms respectively have the more low values and, for these reasons, they are H atoms that quickly form H bonds in solution. These results are in agreement with the analyzed MEP values.

3.3. NBO and AIM studies

The stabilities of all isomers of ribavirin in gas and aqueous solution phases were studied by NBO [53,54] and AIM [55,56] calculations at the B3LYP/6-31G* level of theory in order to analyze the influence of the ribofuranosyl and triazole rings and of the carboxamide groups on the stabilization energies of all structures. **Table 8** shows the results for all isomers.

Table 9. Main delocalization energy (in kJ/mol) for all isomers of ribavirin in both media.

Delocalization	GAS				
	C1	C2	C3	C4	C5
σ (2)C1-N6 → σ(2)C2-N5*	139.15	129.54	132.67	134.39	137.35
σ (2)C2-N5 → σ(2)C1-N6*	42.97	45.6	44.85	43.97	44.68
σ (2)C2-N5 → σ(2)C7-O8*	42.8	46.06	46.52	45.06	46.48
ΔET$_{\pi\rightarrow\pi^*}$	**224.92**	**221.2**	**224.04**	**223.42**	**228.51**
LP(1)N3 → σ(2)C1-N6*	207.79	198.09	201.14	204.07	204.31
LP(1)N3 → σ(2) C2-N5*	114.28	112.61	113.95	112.61	116.10
LP(1)N3 → σ(1)C12-O14*	16.97	37.62	19.85	42.68	-
LP(2)O8 → σ(1)C2-C7*	95.51	94.76	94.05	94.84	93.59
LP(2)O8 → σ(1)C7-N9*	105.38	105.75	105.75	106.05	105.75
LP(1)N9 → σ(2)C7-O8*	259.74	259.54	253.6	253.18	255.10
LP(2)O14 → σ(1)N3-C12*	48.15	16.13	45.69	44.06	47.78
LP(2)O23→ σ(1) C12-C13*	43.76	44.22	49.28	43.93	44.73
ΔET$_{n\rightarrow\pi^*}$	**891.58**	**868.72**	**883.31**	**901.42**	**867.36**
σ(2)C2-N5→ σ*(2)C7-O8*	268.65	294.1	310.49	292.6	313.67
ΔET$_{\pi^*\rightarrow\pi^*}$	**268.65**	**294.1**	**310.49**	**292.6**	**313.67**
ΔE$_{Total}$	**1385.15**	**1384.02**	**1417.84**	**1417.44**	**1409.54**

PCM					
Delocalization	C1	C2	C3	C4	C5
σ (2)C1-N6 → σ(2)C2-N5*	141.03	130.42	135.14	135.39	137.15
σ (2)C2-N5 → σ(2)C1-N6*	42.68	46.52	44.85	43.93	45.39
σ (2)C2-N5 → σ(2)C7-O8*	44.18	47.74	48.32	46.61	48.11
ΔET$_{\pi\rightarrow\pi^*}$	**227.89**	**224.68**	**228.31**	**225.93**	**230.65**
LP(1)N3 → σ(2)C1-N6*	212.59	205.82	208.96	209.04	209.58
LP(1)N3 → σ(2) C2-N5*	113.49	113.49	114.82	111.94	115.74
LP(1)N3 → σ(1)C12-O14*	15.72	34.23	12.71	41.38	4.14
LP(2)O8 → σ(1)C2-C7*	87.15	86.4	85.65	86.32	85.52
LP(2)O8 → σ(1)C7-N9*	95.51	95.43	95.6	95.68	95.55
LP(1)N9 → σ(2)C7-O8*	280.31	279.6	278.93	279.14	278.85
LP(2)O14 → σ(1)N3-C12*	46.36	33.23	49.95	38.00	41.30
LP(2)O23→ σ(1) C12-C13*	41.09	40.67	46.77	40.88	40.71
ΔET$_{n\rightarrow\pi^*}$	**892.22**	**888.87**	**893.39**	**902.38**	**871.39**
σ(2)C2-N5→ σ*(2)C7-O8*	331.1	365.71	409.39	381.84	403.54
ΔET$_{\pi^*\rightarrow\pi^*}$	**331.1**	**365.71**	**409.39**	**381.84**	**403.54**
ΔE$_{Total}$	**1451.21**	**1479.26**	**1531.09**	**1510.15**	**1274.93**

Three important contributions of the stabilization energies to the total energies are observed in all isomers which are the $\Delta ET_{\pi\rightarrow\pi^*}$, $\Delta ET_{n\rightarrow\pi^*}$ and $\Delta ET_{\pi^*\rightarrow\pi^*}$ charge transfers corresponding to the C-N bonds of the triazole rings and to the lone pairs of the N3, N9, O8, O14 and O23 atoms belonging to the pyrimidine and ribofuranosyl rings of all isomers, presenting the $\Delta ET_{\pi\rightarrow\pi^*}$ and $\Delta ET_{n\rightarrow\pi^*}$ charge transfers in the C5 and C4 isomers the higher values in both media while the higher values in the $\Delta ET_{\pi^*\rightarrow\pi^*}$ charge transfers are observed in the C5 and C3 isomers in gas phase and in solution, respectively. Note that in solution, all the charge transfers increase their values, as expected because the atoms involved in these interactions are implicated in the H bonds formation. Here, the total stabilization energy could justify the higher solvation energy observed for C2 and the probable existence of C3 in solution.

The topological properties for all isomers were also studied in both media by using AIM [55,56] calculations in order to investigate the intra-molecular interactions involved in the two rings and in the carboxamide groups. Thus, the electron charge density, (ρ) and the Laplacian of the electron density, $\nabla^2\rho(r)$, the eigenvalues $(\lambda 1, \lambda 2, \lambda 3)$ of the Hessian matrix and the $\lambda 1/\lambda 3$ ratio in the bond critical points (BCPs) and the ring critical points (RCPs) were calculated at B3LYP/6-31G* level and the results can be seen from **Tables 10** to **14**. The $\lambda 1/\lambda 3$ ratio allows the description of the character of interaction between atoms because when $\lambda 1/\lambda 3 > 1$ and $\nabla^2\rho(r) < 0$ the interaction is typical of covalent bonds (called shared interaction) with high values of $\rho(r)$ and $\nabla^2\rho(r)$ while when $\lambda 1/\lambda 3 < 1$ and $\nabla^2\rho(r) > 0$ the interaction is called closed-shell interaction and is typical of ionic, highly polar covalent and hydrogen bonds as well as of the van-der-Waals and specific intermolecular interactions [58-63]. Table 10 shows for C1 in gas phase three BCPs, the O25---H27, N5---H29 and O18---H10 interactions and five RCPs while in C2 only one in gas phase (O25---H27) while in C2 there are two BCPs (H4--H24 and O25--H27) and five RCPs. Thus, the stability of C2 increases in solution. For C3 in both media are observed two BCPs (H4--H24 and O25--H27) and five RCPs solution while only one BCP is expected for C4 in both media. Table 14 shows two BCPs (H18--H4 and O25--H27) and four RCPs in C5. The topological properties of the ribofuranosyl ring of all isomers (RCP1) present the higher changes in relation to the triazole rings (RCP2) but the values are lower for C3 than the other ones. This analysis clearly shows that C1, C2, C3 and C5 due to their stabilities could be expected in gas phase and in solution and, for these reasons, the B3LYP/6-31G* force fields and frequencies calculations for ribavirin in both media could be calculated by using all those structures but, here, only those two C2 and C5 structures experimentally observed in the solid phase are considered in the vibrational study.

Table 10. Analysis of the topological properties for the C1 isomer of ribavirin in both by using the hybrid B3LYP level of theory.

Parameter	Gas phase							
(a.u.)	RPC1	RPC2	O25--H27	RPC3	N5--H29	RCP4	O18--H10	RCP5
$\rho(r_c)$	0.0582	0.0389	0.0241	0.0216	0.0220	0.0105	0.0059	0.0057
$\nabla^2\rho(r_c)$	0.4824	0.2772	0.0916	0.1264	0.0672	0.0404	0.0248	0.0260
λ_1	-0.0732	-0.0428	-0.0291	-0.0208	-0.0272	-0.0083	-0.0061	-0.0051
λ_2	0.2691	0.1555	-0.0231	0.0331	-0.0251	0.0170	-0.0031	0.0040
λ_3	0.2863	0.1644	0.1438	0.1142	0.1197	0.0317	0.0340	0.0273
$\lvert\lambda_1\rvert/\lambda_3$	0.2557	0.2603	0.2024	0.1821	0.2272	0.2618	0.1794	0.1868
Parameter	Aqueous Solution							
(a.u.)	RPC1	RPC2	O25--H27	RPC3	N5--H29	RCP4		
$\rho(r_c)$	0.0584	0.0389	0.0233	0.0212	0.0204	0.0093		
$\nabla^2\rho(r_c)$	0.4836	0.2768	0.0856	0.1192	0.0604	0.0368		
λ_1	-0.0736	-0.0426	-0.0283	-0.0209	-0.0250	-0.0074		
λ_2	0.2668	0.1553	-0.0213	0.0304	-0.0238	0.0154		
λ_3	0.2903	0.1643	0.1352	0.1098	0.1093	0.0288		
$\lvert\lambda_1\rvert/\lambda_3$	0.2742	0.2593	0.2093	0.1903	0.2287	0.2569		

Table 11. Analysis of the topological properties for the C2 isomer of ribavirin in both by using the hybrid B3LYP level of theory.

Parameter	Gas phase			
(a.u.)	RPC1	RPC2	O25--H27	RPC3
$\rho(r_c)$	0.0579	0.0388	0.0219	0.0205
$\nabla^2\rho(r_c)$	0.4804	0.2732	0.0848	0.1144
λ_1	-0.0727	-0.0427	-0.0253	-0.0195
λ_2	0.2660	0.1536	-0.0181	0.0253
λ_3	0.2871	0.1625	0.1284	0.1087
$\lvert\lambda_1\rvert/\lambda_3$	0.2532	0.2628	0.1970	0.1794

	Aqueous Solution						
Parameter	RPC1	RPC2	O25--H27	RPC3	H4--H24	RCP9	RCP10
$\rho(r_c)$	0.0583	0.0387	0.0214	0.0201	0.0045	0.0032	0.0035
$\nabla^2\rho(r_c)$	0.4824	0.2736	0.0820	0.1104	0.0164	0.0112	0.0136
λ_1	-0.0733	-0.0430	-0.0249	-0.0194	-0.0036	-	-0.0015
λ_2	0.2655	0.1543	-0.0173	0.0241	-0.0033	0.0048	0.0048
λ_3	0.2901	0.1624	0.1242	0.1056	0.0232	0.0070	0.0104
$\lvert\lambda_1\rvert/\lambda_3$	0.2527	0.2648	0.2005	0.1837	0.1552	0.0714	0.1442

Table 12. Analysis of the topological properties for the C3 isomer of ribavirin in both by using the hybrid B3LYP level of theory.

Parameter	Gas phase					
(a.u.)	RPC1	RPC2	O25-	RPC3	O25-H4	RCP6
$\rho(r_c)$	0.0580	0.0380	0.0205	0.0197	0.0092	0.0058
$\nabla^2\rho(r_c)$	0.4808	0.2704	0.0812	0.1060	0.0352	0.0264
λ_1	-0.0728	-0.0423	-0.0233	-0.0189	-0.0090	-0.0026
λ_2	0.2659	0.1528	-0.0146	0.0198	-0.0062	0.0062
λ_3	0.2877	0.1598	0.1193	0.1052	0.0505	0.0227
$\lvert\lambda_1\rvert/\lambda_3$	0.2530	0.2647	0.1953	0.1797	0.1782	0.1145
	Aqueous Solution					

Parameter	RPC1	RPC2	O25-	RPC3	O25-H4	RCP6
$\rho(r_c)$	0.0584	0.0381	0.0236	0.0214	0.0075	0.0058
$\nabla^2\rho(r_c)$	0.4832	0.2704	0.0868	0.1204	0.0296	0.0252
λ_1	-0.0735	-0.0424	-0.0289	-0.0212	-0.0065	-0.0027
λ_2	0.2664	0.1532	-0.0219	0.0313	-0.0030	0.0049
λ_3	0.2905	0.1595	0.1375	0.1103	0.0393	0.0231
$\lvert\lambda_1\rvert/\lambda_3$	0.2530	0.2658	0.2102	0.1922	0.1654	0.1169

Table 13. Analysis of the topological properties for the C4 isomer of ribavirin in both by using the hybrid B3LYP level of theory.

Parameter	Gas phase			
(a.u.)	RPC1	RPC2	O25-H27	RPC3
$\rho(r_c)$	0.0581	0.0387	0.0239	0.0216
$\nabla^2\rho(r_c)$	0.4812	0.2764	0.0880	0.1232
λ_1	-0.0730	-0.0426	-0.0290	-0.0211
λ_2	0.2662	0.1557	-0.0224	0.0322
λ_3	0.2880	0.1632	0.1395	0.1122
$\lvert\lambda_1\rvert/\lambda_3$	0.2535	0.2610	0.2079	0.1880
Parameter	Aqueous Solution			
(a.u.)	RPC1	RPC2	O25-H27	RPC3
$\rho(r_c)$	0.0584	0.0390	0.0211	0.0200
$\nabla^2\rho(r_c)$	0.4828	0.2768	0.0800	0.1076
λ_1	-0.0735	-0.0428	-0.0245	-0.0194
λ_2	0.2656	0.1560	-0.0166	0.0231
λ_3	0.2909	0.1637	0.1211	0.1040
$\lvert\lambda_1\rvert/\lambda_3$	0.2527	0.2614	0.2023	0.1865

Table 14. Analysis of the topological properties for the C5 isomer of ribavirin in both by using the hybrid B3LYP level of theory.

Parameter	Gas phase					
(a.u.)	RCP1	RCP2	018--H4	RCP7	O25-H27	RCP8
$\rho(r_c)$	0.058	0.0387	0.0081	0.0058	0.0259	0.0225
$\nabla^2\rho(r_c)$	0.4820	0.2756	0.0296	0.0260	0.0972	0.1348
λ_1	-0.0728	-0.0428	-0.0081	-0.0037	-0.0321	-0.0218
λ_2	0.2648	0.1536	-0.0073	0.0124	-0.0263	0.0376
λ_3	0.2899	0.1648	0.0451	0.0174	0.1557	0.1191
$\lvert\lambda_1\rvert/\lambda_3$	0.2511	0.2597	0.1796	0.2126	0.2062	0.1830
Parameter	Aqueous Solution					
(a.u.)	RCP1	RCP2	O18-H4	RCP7	O25-H27	RCP8
$\rho(r_c)$	0.0585	0.0388	0.0062	0.0049	0.0220	0.0205
$\nabla^2\rho(r_c)$	0.4840	0.2756	0.0232	0.0224	0.0840	0.1140
λ_1	-0.0735	-0.0430	-0.0060	-0.0027	-0.0258	-0.0197
λ_2	0.2654	0.1543	-0.0052	0.0089	-0.0185	0.0260
λ_3	0.2921	0.1642	0.0343	0.0163	0.1284	0.1077
$\lvert\lambda_1\rvert/\lambda_3$	0.2516	0.2619	0.1749	0.1656	0.2009	0.1829

3.4. HOMO-LUMO and descriptors of ribavirin

The reactivity and behaviour of ribavirin were predicted in both media in order to know the nature of the interactions with electrophiles and/or nucleophiles because the presence of ribofuranosyl and triazole rings and of the carboxamide groups in this species confer to it its antiviral properties. Therefore, for all isomers, the HOMO and LUMO orbitals, energy band gap, chemical potential (μ), electronegativity (χ), global hardness (η), global softness (S) and global electrophilicity index (ω) descriptors were calculated in both phases by using the B3LYP/6-31G* method. The results and the equations used to compute the descriptors can be seen in **Table 15** while the gap and descriptors values corresponding to other antiviral agents with different structures in **Table 16** are presented [14,46-48]. The comparisons are very interesting taking into account that all these compounds have five and six member's rings in their structures. Comparing the energy band gaps for both conformers of ribavirin, we observed that C1 has the lowest gap for which is the most reactive isomer in both media while C5 is the less reactive in both media. When these values are compared with those reported for thymidine [14], zalcitabine [46] and trifluoromethyluracyl (TFMU) [47], we observed that all isomers of ribavirin present values similar to TFMU but notably different from cidofovir and brincidofovir [48]. Here, it is very important to mention that the gap value observed for C5 is similar to that value obtained for ribavirin by using B3LYP/6-311++G** calculations by Rizwana et al [22].

Table 15. Calculated HOMO and LUMO orbitals. energy band gap. chemical potential (μ). electronegativity (χ). global hardness (η). global softness (S). global electrophilicity index (ω) and global nucleophilicity index (E) for the most stable isomers of ribavirin at B3LYP/6-31G* level of theory.

Gas phase					
Orbitals [eV]	C1	C2	C3	C4	C5
HOMO (64)	-6.7958	-6.6991	-6.6134	-6.7501	-6.5337
LUMO (65)	-0.9530	-0.7560	-0.6227	-0.8380	-0.5205
|GAP|	-5.8428	-5.9431	-5.9907	-5.9121	-6.0132
Descriptors					
χ = - [E(LUMO)- E(HOMO)]/2	-2.9214	-2.9716	-2.9953	-2.9560	-3.0066
μ = [E(LUMO) + E(HOMO)]/2	-3.8744	-3.7276	-3.6180	-3.7940	-3.5271
η = [E(LUMO) – E(HOMO)]/2	2.9214	2.9716	2.9953	2.9560	3.0066
S = ½η (eV)	0.1712	0.1683	0.1669	0.1691	0.1663
ω = μ^2/2η (eV)	2.5691	2.3379	2.1851	2.4348	2.0688
ε = μ η	-11.3187	-11.0766	-10.8370	-11.2151	-10.6046
Aqueous Solution					
HOMO (64) (a.u.)	-6.6909	-6.5623	-6.4164	-6.5685	-6.3560
LUMO (65) (a.u.)	-0.9510	-0.7435	-0.5260	-0.7686	-0.4484
|GAP|	-5.7399	-5.8188	-5.8904	-5.7999	-5.9076
Descriptors					
χ = - [E(LUMO)- E(HOMO)]/2	-2.8700	-2.9094	-2.9450	-2.8999	-2.9538
μ = [E(LUMO) + E(HOMO)]/2	-3.8210	-3.6529	-3.5012	-3.6685	-3.4022
η = [E(LUMO) – E(HOMO)]/2	2.8700	2.9094	2.9450	2.8999	2.9538
S = ½η (eV)	0.1742	0.1719	0.1698	0.1724	0.1693
ω = μ^2/2η (eV)	2.5435	2.2932	2.0812	2.3204	1.9593
ε = μ η	-10.9659	-10.6277	-10.3110	-10.6383	-10.0494

Obviously, the presence of the oxopyrimidin rings together to the oxymethylphosphonic and oxymethyl-(3-hexadecoxypropoxy)phosphinic acid side chains in cidofovir and brincidofovir generate a notable decreasing in the gap values and, for these reasons, both cidofovir and brincidofovir species present higher reactivities than ribavirin. Analyzing the descriptors of ribavirin, we observed that in accordance with their reactivities C1 present lower chemical hardness η than the other ones in both media while when the values are compared with the

corresponding to the antiviral thymidine [14], zalcitabine [46] and trifluoromethyluracyl [47] the values are similar among them but different from brincidofovir [48].

Evidently, the large side chain together with the presence of the oxymethylphosphonic ring increase the reactivity of brincidofovir because modify their chemical properties, as reported by Romani and Brandán [48]. The effect of the different groups and rings in the structures have influence on both global electrophilicity ω and nucleophilicity ε index values, as observed in Tables 15 and 16. Thus, the uracil ring and the CF_3 groups in TFMU and the oxymethylphosphonic ring and the large -$(CH_2)_3$-O-$(CH_2)_{15}$-CH_3) side chain in brincidofovir generate the higher ω values, however, the higher ε values are observed for both conformers of ribavirin and TFMU. Thus, the ω values decreasing in the following order: TFMU > brincidofovir > ribavirin > zalcitabine > thymidine > cidofovir while the ε values decrease according the order: TFMU > ribavirin > thymidine > zalcitabine > cidofovir > brincidofovir. This study shows: (i) that a molecule with two five members ring (ribavirin) has lower reactivity than those with a six members ring (cidofovir, brincidofovir, TFMU) or those with two different rings of five and six members as thymidine and zalcitabine and (ii) that the presence of a CF_3 group in the structure of a antiviral agent decrease their reactivity but increase the electrophilicity and nucleophilicity index values.

Table 16. Calculated HOMO and LUMO orbitals, energy band gap, chemical potential (μ), electronegativity (χ), global hardness (η), global softness (S), global electrophilicity index (ω) and global nucleophilicity index (E) for some antiviral agents at B3LYP/6-31G* level of theory.

B3LYP/6-31G*					
Orbitals	Zalcitabine[a]	thymidine[b]	TFMU[c]	Cidofovir[d]	Brincidofovir[d]
HOMO	-6.1138	-6.1061	-7.5234	-5.9366	-5.9366
LUMO	-0.7543	-0.6313	-1.7132	-0.6401	-1.772
|GAP|	-5.3595	-5.4748	-5.8102	-5.2965	-3.7715
Descriptors					
χ	-2.6798	-2.7374	-2.9051	-2.6483	-1.8858
μ	-3.4341	-3.3687	-4.6183	-3.2884	-3.6578
η	2.6798	2.7374	2.9051	2.6483	1.8858
S	0.1866	0.1827	0.1721	0.1888	0.2651
ω	2.2003	2.0728	3.6709	2.0416	3.5474
ε	-9.2024	-9.2215	-13.4166	-8.7084	-6.8976

[a]From Ref [46], [b]From Ref [14],[c]From Ref [47],[d]From Ref [48]

3.5. Vibrational analysis

Experimentally, only the structures of two C2 and C5 isomers were observed by X-ray diffraction in solid phase [50] and both were predicted by calculations, for these reasons, in this analysis we have considered those two optimized structures. The available experimental infrared spectrum for ribavirin in solid phase was taken from Ref [19] while the Raman spectrum used was that available from the literature [22]. Both spectra are compared with the corresponding predicted for C2 and C5 calculated in gas phase by using the B3LYP/6-31G* method in **Figures 7** and **8**, respectively. For both conformers are expected 81 normal vibration modes where all the modes are active in the IR and Raman spectra. The predicted spectra for C2 and C5 show some bands most intense than the experimental one, however, resulting IR spectrum for a population relation C2:C5 of 1:1 for each isomer reproduces better some bands of experimental spectrum, as indicated in **Figure 9**.

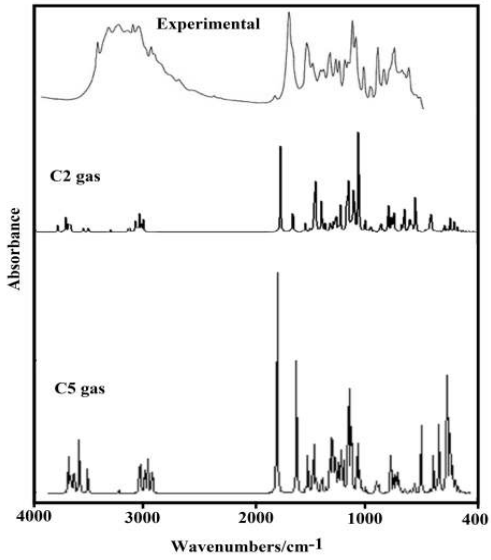

Figure 7. Experimental infrared spectrum in the solid state of ribavirin taken from Ref [19] compared with the corresponding predicted for C2 and C5 conformers by using B3LYP/6-31G* level of theory.

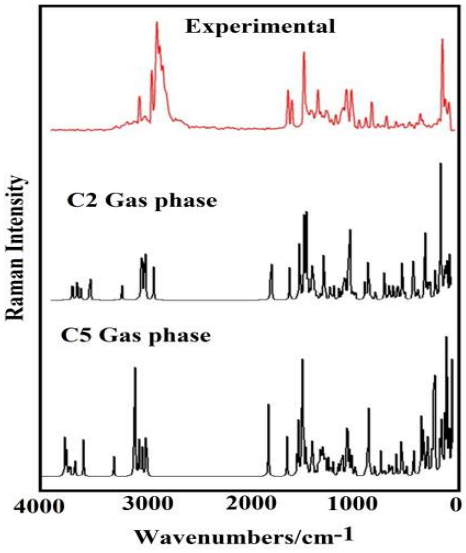

Figure 8. Experimental Raman spectrum in the solid state of ribavirin taken from Ref [22] compared with the corresponding predicted for C2 and C5 conformers by using B3LYP/6-31G* level of theory.

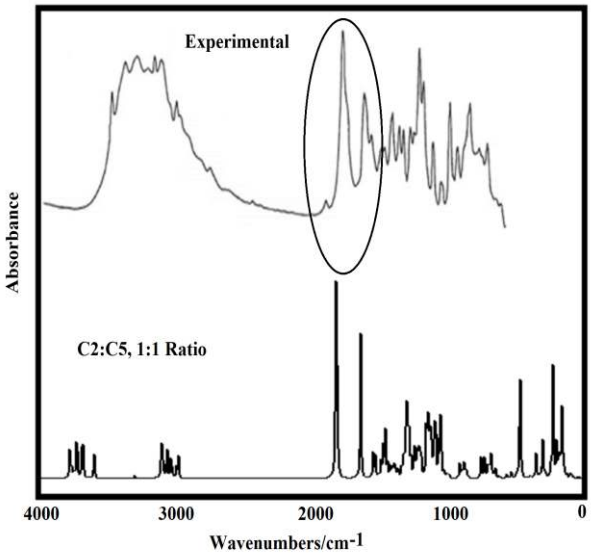

Figure 9. Comparison between the infrared experimental spectrum of ribavirin with the calculated infrared spectra for C2 and C5 isomers from B3LYP/6–31G∗ wavenumbers and intensities using Lorentzian band shapes (for a population relation C2:C5 of 1:1 for each isomer).

In **Table 17** are summarized the experimental and calculated wavenumbers for all the normal vibration modes of C2 and C5 in both media by using 6-31G* basis set together to the corresponding assignments. These assignments were performed taking into account the results of the SQM/B3LYP/6-31G* calculations, previous assignments [22] and assignments reported for antiviral agents with similar groups [14-18,46-48]. In general, in the IR spectra in solution some bands are enlarged and shifted toward lower wavenumbers as consequence of the hydration of the OH groups, as also was observed for thymidine [14]. The displacement of the bands as a consequence of hydration can be easily seen in Table 17 and, in particular, those bands associated to the C=O stretching modes due to the H bonds. Here, the differences observed between the experimental spectra registered in solid phase and the corresponding predicted could be attributed to the calculations performed in gas phase where the molecules are isolated while in the solid phase the crystal packing forces are important and, they were not considered here. Below, we have discussed the assignments for some vibration modes.

Table 17. Observed and calculated wavenumbers (cm^{-1}) and assignments for the C2 and C5 isomers of ribavirin in gas phase and in aqueous solution

IR[b]	Ra[c]	C2[a]				C5[a]			
		Gas phase		Aqueous solution		Gas phase		Aqueous solution	
		SQM[d]	Asignment	SQ	Asignment	SQ	Asignment	SQM[e]	Asignment
		3614	νO25-H28	359	νO25-H28	361	νO25-H28	3593	νO25-H28
3449s		3575	ν_aNH_2	355	νO18-H29	359	νO18-H29	3586	νO18-H29
		3567	νO18-H29	354	ν_aNH_2	357	ν_aNH_2	3541	ν_aNH_2
		3533	νO23-H27	351	νO23-H27	352	νO23-H27	3503	νO23-H27
3347	3247w	3449	ν_sNH_2	343	ν_sNH_2	344	ν_sNH_2	3424	ν_sNH_2
3257	3124m	3147	νC1-H4	317	νC1-H4	316	νC1-H4	3176	νC1-H4
3164sh	3072w			299	νC13-H19			2997	νC13-H19
3117	3009s			299	ν_aCH_2(C17)			2989	νC16-H21
3066w		2972	νC12-H22	299	νC12-H22			2984	νC12-H22
2997sh		2966	ν_aCH_2(C17)	297	νC16-H21	297	νC13-H19	2977	νC15-H20
		2956	νC13-H19	297	νC15-H20	297	νC12-H22		
2950s	2957vs	2933	νC16-H21			296	νC16-H21		
2916sh	2929s	2929	νC15-H20			293	νC15-H20	2942	ν_aCH_2(C17)
	2901s			290	ν_sCH_2(C17)	290	ν_aCH_2(C17)	2906	ν_sCH_2(C17)
2880sh	2877sh	2851	ν_sCH_2(C17)			286	ν_sCH_2(C17)		
1657vs	1659m	1749	νC7=O8	1812	$wagNH_2$	1746	νC7=O8	1663	νC7=O8,δNH$_2$
1639sh	1627m	1562	δNH_2	164	νC7=O8	156	δNH_2	1624	$wagNH_2$
1494	1508s	1489	νN6-C1			147	δCH_2		
1473sh	1488sh			147	νN6-C1	147	νN6-C1	1471	$wagNH_2$,δN
		1460	δCH_2	144	δCH_2			1465	$wagCH_2$
1437w	1436w			144	ρC12-H22	144	$wagCH_2$	1448	δCH_2
1437w	1436w	1441	νC2-C7	143	ρC13-H19	143	νC2-C7	1443	$wagNH_2$,δN
		1430	ρC12-H22	142	$wagCH_2$			1430	ρC13-H19
		1420	$wagCH_2$	1421	$wagCH_2$,δNH$_2$	1417	ρC13-H19	1422	$wagNH_2$,δNH$_2$
		1405	ρC13-H19,δO23-H27			1407	ρC12-H22		
	1382sh	1389	δC15C13O23	139	δC15C13O2	139	δC15C13O2	1395	ρC15-H20
1386sh	1373m	1374	νN3-C12	137	νN5-C2			1370	ρC16-H21
		1363	ρC16-H21,ρCH_2	136	ρCH_2	136	ρC16-H21	1368	νN5-C2
1364w	1352sh	1356	νN5-C2	1358	δO23-H27	1349	ρC12-H22,		
1342 w		1335	δO18-H29	1342	ρ´C13-H19	1341	νN5-C2,νN6-C2	1348	δO23-H27
	1320w	1326	ρC16-H21	1334	ρC16-H21	1315	ρ´C12-H22	1329	ρC12-H22,
				131	ρ´C13-H19			1299	ρ´C16-H21
1294 sh	1288w	1289	ρ´C13-H19	128	ρ´C12-H22	129	ρ´C16-H21	1297	ρ´C13-H19
1277	1268sh	1275	ρ´C12-H22	127	ρ´C15-H20	127	ρ´C13-H19	1282	ρ´C15-H20
1274 sh		1264	ρ´C16-H21			127	ρ´C15-H20	1266	ρ´C12-H22
		1261	νN6-C2,νN9-C7	126	ρ´C16-H21	125	νN9-C7	1251	ρCH_2,wagN
		1245	ρC13-H19,ρ´C12-H22			1249	ρC13-H19,	1246	ρCH_2
1237 sh				123	$wagCH_2$,δN	123	ρCH_2		

1220	1233w					122	νN3-N5		
1213 sh		1202	βC1-H4	120	νC13-O23			1208	νN3-N5
1193w	1193w	1193	ρCH_2	119	δO18-H29			1204	νC13-O23
		1191	νN3-N5	119	νN3-N5	119	δO18-H29	1196	δO18-H29
1183sh						118	βC1-	1172	νO14-C12
				116	βC1-H4			1166	βC1-H4
1147sh	1147sh	1155	δO25-H28	115	δO25-H28				
1137						114	δO25-H28	1140	δO25-H28
1129sh	1121sh	1113	νC13-O23						
1111w	1105sh			109	νO14-C12	110	νC13-O23		
1085sh	1089s	1086	νC16-C17			109	νO14-C12		
1067vs	1073sh	1073	νC17-O18	107 7	νN9-C7	108 0	νC15-O25	1071	νC15-O25
1067vs		1072	νN9-C7	107 3	νC15-O25	107 2	νN9-C7	1067	ρNH_2,
1061sh		1060	νC12-C13	106 2	νC16-C17	105 6	νC17-O18	1050	νC16-C17
1035s	1041s	1043	νC17-O18	104	νC15-O25	103	νN3-C1	1042	νC12-C13
1035s		1036	νC15-C16	102 4	νN3-C1,	103 1	νC12-C13	1027	$\beta R_2(A_2)$,
1035s	1024sh	1020	νO14-C12			101	νC16-C17	1023	νC15-C16
1016sh	1014sh	1000	νC15-O25	101 4	νC17-O18	100 3	$\beta R_2(A_2)$,$\beta R_1($ $A_2)$		
	1002vw	996	$\beta R_2(A_2)$,$\beta R_1(A_2)$	986	νC17-O18	989	τwCH_2	986	$\beta R_1(A5_2)$
972sh	960w			978	$\beta R_1(A_2)$,$\beta R_2($			984	νC17-O18
957	948sh	955	νO14-	944	τwCH_2	951	νC15-C16	953	τwCH_2
911sh								908	γC1-H4
896	894w	871	νC13-C15	872	νC13-C15	879	γ C1-H4		
		851	δN3C12C13	863	γC1-H4			859	νC13-C15
849sh	839s	835	γC1-H4			846	δN3C12C13,		
828s	839s	826	νO14-	834	δN3C12C13	837	νC13-C15	836	δN3C12O14
819sh	825sh			811	νO14-C16	825	νO14-C16	813	νO14-C16
771w	777w	792	γC7=C8	788	$wagCH_2$,δN	792	γC7=C8	785	$wagNH_2$,δN
720sh	733w			723	$\beta R_1(A_1)$	735	$\beta R_1(A_1)$	729	$\beta R_1(A_1)$
690sh	695w	708	$\beta R_1(A_1)$			707	$\beta R_2(A_1)$, δN3C12O14		
673m	677sh			670	$\tau R_1(A_2)$,γC7=	670	$\tau R_1(A_2)$	682	$\beta R_2(A_1)$
667sh		666	βC7=O8	668	$wagCH_2$,δN	661	βC7=O8	665	γC7=C8
		662	$\tau R_1(A_2)$	665	$wagCH_2$,δN			664	βC7=O8,$\tau R_1($
	650vw	650	$\tau R_2(A_2)$						
630sh		630	$\tau R_2(A_2)$	638	$\tau R_2(A_2)$	635	$\tau R_2(A_2)$	642	$\tau R_2(A_2)$
609w	600w			611	$\beta R_2(A_1)$	603	δC15C13O2 3,	609	δC15C13O2 3
584w	586sh	591	$\beta R_2(A_1)$						

571w	554sh	554	δC17C16O14	556	δC17C16O14	554	βC2-C7	557	βC2-C7
537w	532w	531	δC17C16O14	530	τwNH$_2$	516	δC17C16O14	518	δC17C16O14
478sh	467w	510	τwNH$_2$	525	τwNH$_2$,wag	514	τwNH$_2$	507	τwNH$_2$
443sh	437w	431	δC12C13O23	432	δC2C7N9,	436	δC2C7N9	433	δC2C7N9
421sh		423	δC2C7N9 τO23-H27,	426	βC7=O8,νC δC12C13-O23				νC2-C7
413sh		416	τO18-H29			416	τO23-H27		
413sh	409sh	414	τO23-H27					407	δN3C12C13
	397w			389	τO23-H27	393	δN3C12C13	384	δC12C13O2
	370sh			379	τO23-H27	375	δC12C13O2	368	τO23-H27
	359m	358	νC15-C16	350	τO18-H29			348	β N3-C12
				342	δN3C12O14	341	δC12C13-O23		
	337sh	339	δC16C15O25			337	δC16C15O2		
	314sh	317	δC17C16O14					322	δC17C16O14
				305	δC16C15O2	308	δC15C13O2		
	276w	279	δC13C15O25	279	δNH$_2$,wagNH$_2$	281	δC16O17O18	288	δC12C13O23
		268	δC12C13O23	260	δC13C15O2	262	τO18-H29	260	δC13C15O2
	232sh	230	δN3C12O14	235	δNH$_2$wagNH$_2$	232	δN3C12O14	237	τO18-H29
	218w			225	δNH$_2$,wagN			225	δNH$_2$,wagN
		199	τO25-H28	197	δNH$_2$,wagN	216	wagNH$_2$	195	γC2C7
	190sh					189	γC2C7	194	δC15C16C17
	176w	185	γC2-C7	186	δC15C16C17	187	δC15C16C17	184	δNH$_2$,
	158sh	168	δC15C16C17			156	τO25-H28	173	τO25-H28
	142vs	152	wagNH$_2$	149	τO25-H28			142	τR$_2$(A$_1$)
	142vs			133	τC16-C17	135	τR$_2$(A$_1$),		
	114sh	126	βC2-C7,βN3-C12	122	βN3-C12	107	τC16-C17,	120	βN3-C12,
	102sh	108	τC16-C17	100	γN3-C12			92	τC16-C17
	75sh	84	γN3-C12	83	τR$_1$(A$_1$)	83	γN3-C12	79	γN3-C12
		66	τR$_2$(A$_1$),τR$_1$ (A$_1$)			67	τR$_2$(A$_1$)		
	55sh			57	τwC2-C7	56	τR$_1$(A$_1$)	53	τR$_1$(A$_1$)
		35	τwC2-C7	46	τwN3-C12	37	τwC2-C7	39	τwC2-C7

28	$\tau R_2(A_1),\tau R_1(A_1)$	26	$\tau R_2(A_1)$			31	τwN3-C12
8	τwN3-C12			17	τwN3-C12		

ν, stretching; δ, scissoring; wag, wagging or out- of plane deformation; ρ, rocking; τ, torsion, twist, twisting; a, antisymmetric; s, symmetric ; ip, in-phase; op, out-of-phase; R, ring; A1, triazole ring; A2, sugar ring.

[a]This work, [b]From Ref [19], [c]From Ref [22], [d]From scaled quantum mechanics force field B3LYP/6-31G*, [e]From scaled quantum mechanics force field PCM/B3LYP/6-31G*

3.5.1. Assignments

3.5.1.1. OH modes. In both C2 and C5 isomers of ribavirin, three OH stretching modes are expected. Hence, the strong and broad IR band at 3449 cm^{-1} can be associated to the OH stretching modes of deoxyribose ring, because these modes are predicted by SQM calculations between 3618 and 3503 cm^{-1}, as observed in Table 17 and as was reported for thymidine [14,18]. Note that these modes in solution are slightly predicted toward lower wavenumbers, as a consequence of hydration. The OH in-plane deformation modes were predicted between 1358 and 1073 cm^{-1}, hence, these modes are assigned to the bands observed in this region, as was observed in similar compounds [14-18,33,35-39,41,46-48]. In isomers of thymidine these modes were assigned to IR bands observed between 1288 and 1173 cm^{-1} [14,18] while the out-of-plane deformation modes or torsion modes were predicted by calculations between 423 and 149 cm^{-1}. Then, these modes were assigned accordingly.

3.5.1.2. CH modes. The only aromatic C1-H4 stretching modes belonging to the triazole rings of both isomers of ribavirin are predicted by SQM calculations at higher wavenumbers than the corresponding to deoxyribose rings and, obviously, they are clearly assigned to the Raman band of the medium intensity at 3124 cm^{-1}. The aliphatic C-H stretching modes belonging to the deoxyribose rings are predicted between 2999 and 2939 cm^{-1}, for which, they were assigned, as detailed in Table 17. The remaining vibration modes expected for these groups were assigned as predicted by calculations.

3.5.1.3. NH_2 modes. For the C2 and C5 isomers of ribavirin, two antisymmetric and symmetric stretching modes are expected. Here, the antisymmetric modes were predicted in the OH stretching modes region while the symmetric stretching modes were predicted at lower wavenumbers than the OH stretching ones. Thus, the IR bands at 3449 and 3347 cm^{-1} can be easily assigned to these modes, as reported for isomers of emtricitabine [17]. The deformation and rocking modes in isomers of emtricitabine were assigned at 1586 cm^{-1} and 1064/1040 cm^{-1}, respectively while these modes in ribavirin are predicted between 1663 and 1421 cm^{-1} and, for these reasons; they are assigned in this region. In isomers of emtricitabine [17] the twisting modes were assigned between 539 and 503 cm^{-1} while the wagging modes were predicted between 192 and 108 cm^{-1}. Here, the wagging modes were predicted by SQM calculations at higher wavenumbers (1812/1421 cm^{-1}) than the isomers of emtricitabine. In these latter isomers, the wagging modes are strongly shifted at lower wavenumbers due probably to the proximities of NH_2 groups with the C-F bonds [17]. In C2 and C5 of ribavirin the wagging modes are also predicted in different regions and coupled with deformation NH_2 modes (1443/1421/1236/788/668 cm^{-1}).

3.5.1.4. CH_2 modes. The stretching modes in thymidine were predicted by B3LYP calculations between 3034 and 2851 cm^{-1} [14,18] while in ribavirin in both media these modes are predicted in different regions. Hence, these modes in both C2 and C5 isomers are associated to the IR and Raman bands observed between 2993 and 1851 cm^{-1}. Here, the scissoring, wagging, rocking and twisting modes for both isomers of ribavirin were respectively assigned to the IR and Raman bands at 1476/1443, 1465/1420, 1365/1193 and 955/507 cm^{-1}, as predicted by SQM calculations and, as was reported in molecules containing these groups [14-18, 33,35-39,41,46-48].

3.5.1.5. Skeletal modes.

In isomers of thymidine, the C=O stretching modes in gas phase were predicted by SQM calculations at higher wavenumbers than in aqueous solution due probably to their hydrations. In both isomers of ribavirin, these modes are predicted in C2 and C5 in gas phase at 1749 and 1746 cm^{-1}, respectively while in solution are predicted at 1644 and 1663 cm^{-1}. Thus, the intense IR band and the shoulder at 1657 and 1639 cm^{-1} can be assigned to these vibration modes. The N6=C1 stretching modes of triazole rings are predicted by the SQM calculations in both isomers at higher wavenumbers than the corresponding to N6-C2 stretching modes, hence, clearly double bond characters are observed in the N6=C1 bonds while partial double bonds character are predicted for the second ones. The C2-C1 stretching inter-rings are predicted in both C2 and C5 isomers at notably higher wavenumbers (1441/1438 cm^{-1}) than in aqueous solution (432/433 cm^{-1}) and, for these reasons, they are clearly influenced by the hydrations on both NH_2 and C=O groups. Hence, these modes in both isomers of ribavirin are assigned as predicted by calculations. After all, the remaining skeletal modes including deformations and torsions of triazole and deoxyribose rings are assigned, as predicted by calculations and, in accordance to similar species [14-18,46-48].

4. Force fields

The scaled force fields for both isomers of ribavirin at the B3LYP/6-31G* level of theory were used to compute the harmonic force constants in gas and in aqueous solution by using the SQM procedure and the Molvib program [44,45]. The results can be seen in **Table 18** compared with those reported for the most stable C6 isomer of entricitabine [17]. Here, it is necessary to clarify that the force constants of ribavirin were not compared with those constants reported for zalcitabine because its structure has a pyrimidine ring instead triazole ring. In general, it is observed that the *f(O-H), f(νNH₂)* and *f(νC=O)* force constants of ribavirin and emtricitabine isomers present a slight decreasing in solution, in relation to their values calculated in gas phase, probably due to the hydration of the groups involved. The force constants $f(\nu C\text{-}O)_{OH}$ related to the OH groups increase in solution in both isomers of ribavirin while in emtricitabine in the same medium is observed a decrease in the values from 5.27 mdyn $Å^{-1}$ in gas phase to 5.11 mdyn $Å^{-1}$ in solution. Probably, in ribavirin, the increase could be related to higher number of OH groups while in emtricitabine the decrease is attributed to the H bonds formation. On the other hand, the *f(νC-N)* force constant value slightly increases in solution but in both isomers of ribavirin in the same medium decrease their values, in relation to the values in gas phase. Here, the absence of an S atom in the deoxyribose ring could generate those decreases in the values of both isomers of ribavirin.

Table 18. Scaled force constants for the stable conformers of ribivirin in gas and aqueous solution phases

Force constant	B3LYP/6-31G*[a]					
	Ribavirin[a]				Emtricitabine[b]	
	Gas phase		Aqueous solution		Gas phase	Aqueous solution
	C2	C5	C2	C5	C6	C6
f(νO-H)	7.14	7.17	7.07	7.09	7.07	7.09
f(νNH₂)	6.85	6.83	6.75	6.72	6.88	6.80
f(νCH₂)	4.67	4.59	4.75	4.72		
$f(\nu C\text{-}H)_{Fu}$	4.78	4.83	4.90	4.90	4.89	4.97
$f(\nu C\text{-}H)_{Tr}$	5.42	5.47	5.50	5.51	5.41	5.44
f(νC=O)	11.92	11.88	10.40	10.41	11.22	9.81
$f(\nu C\text{-}O)_{Fu}$	4.35	4.67	4.50	4.96	4.54	4.97
$f(\nu C\text{-}O)_{OH}$	5.21	5.15	5.63	5.60	5.27	5.11
$f(\nu C\text{-}N)_{Tr}$	6.97	6.93	6.82	6.81	6.05	6.10
$f(\nu C\text{-}C)_{Fu}$	3.74	3.72	3.83	3.79	3.84	3.89
$f(\nu N\text{-}N)_{Tr}$	5.76	5.85	5.50	5.59		
f(•H-C-H)	0.81	0.83	0.80	0.81		

f(▪C-O-H)	0.76	0.75	0.77	0.75

ν, stretching; ▪▪ angle deformation.

Units in mdyn Å^{-1} for stretching and mdyn Å rad $^{-2}$ for angle deformations

[a]This work, [b]From Ref [17].

Conclusions

In this work, the molecular structures of five stable isomers (from C1 to C5) of antiviral ribavirin agent were theoretically determined in gas and aqueous solution phases by using the hybrid B3LYP/6-31G* method. Here, the solvent effects in aqueous solution were studied with the self consistent reaction field (SCRF) methodology employing the polarized continuum (PCM) and the universal solvation model (SM). The structural, electronic and topological properties were reported for all isomers while the vibrational analyses were performed only for those two polymorphic structures experimentally observed in the solid phase by X-ray diffraction. B3LYP/6-31G* calculations have evidenced that C2 correspond to the polymorphic V1 structure while C5 to the polymorphic V2 structure. Probably, the higher dipole moment values observed for C2 and C5 in both media could explain their presences in the solid phase despite their low populations in both media. Possibly, the low population observed in C2 could be attributed to the proximities between the more electronegative N---O atoms. Here, the 81 vibration modes expected for C2 and C5 in both media were completely assigned. Experimental available infrared and Raman spectra of ribavirin in the solid state and the normal internal coordinated were employed together with the corresponding SQMFF force fields and the Molvib program to perform the complete vibrational assignments in both media. The force constants for C2 and C5 were also obtained and compared with the values reported for the antiviral emtricitabine agent. The most negative solvation energies are evidenced for both C2 and C5 isomers of ribavirin than the other ones. The frontier orbital study reveals that C1 is the most reactive isomer while C5 is the less reactive in both media. All isomers of ribavirin show values similar to antiviral trifluoromethyluracyl but notably different from antivirals cidofovir and brincidofovir. Here, the gap value observed for C5 is in agreement with the value obtained recently for ribavirin by using B3LYP/6-311++G** calculations. The comparisons with antiviral agents show that the electrophilicity index values decreasing in the following order: trifluoromethyluracyl > brincidofovir > ribavirin > zalcitabine > thymidine > cidofovir while the nucleophilicity index values decrease according the order: trifluoromethyluracyl > ribavirin > thymidine > zalcitabine > cidofovir > brincidofovir.

Data Availability (excluding Review articles)

The SQM force fields for all the conformers of ribavirin can be obtained at request.

Conflicts of Interest

Authors declare there are not conflict of interests.

Funding Statement

This work was founded with grants from Project Nº 26/D608 CIUNT (Consejo de Investigaciones, Universidad Nacional de Tucumán).

Acknowledgments

The authors thank Prof. Tom Sundius for his permission to use MOLVIB.

References

1. De Clercq E, Antiviral drugs in current clinical use, Journal of Clinical Virology, 2004; 30: 115–133.

2. Moreno A, Bárcena R, García-Garzón S, Muriel A, Quereda C, Moreno L, Mateos ML, Fortún J, Martín-Dávila P, García M, Blesa C, Otón E, Moreno A, Moreno S, HCV clearance and treatment outcome in genotype 1 HCV-monoinfected, HIV-coinfected and liver transplanted patients on peg-IFN-α-2b/ribavirin, Journal of Hepatology, 2005; 43(5): 783-790.

3. Loustaud-Ratti V, Debette-Gratien M, Jacques J, Alain S, Marquet P, Sautereau D, Rousseau A, Carrier P, Ribavirin: Past, present and future, World J Hepatol, 2016; 8(2): 123-130

4. Galli A, Mens H, Gottwein JM, Gerstoft J, Bukh J, Antiviral Effect of Ribavirin against HCV Associated with Increased Frequency of G-to-A and C-to-U Transitions in Infectious Cell Culture Model, Scientific Reports, 2018; 8: 4619.

5. Zoulim F, Moreno C, Lee SS, Buggisch P, Horban A, Lawitz E, Corbett C, Lenz O, Fevery B, Verbinnen T, Shukla U, Jessner W, A 3-year follow-up study after treatment with simeprevir in combination with pegylated interferon-α and ribavirin for chronic hepatitis C virus infection, Virology Journal, 2018, **15**:26

6. J-M Chen, Song Li, Tong-Bu Lu, Pharmaceutical Cocrystals of Ribavirin with Reduced Release Rates, *Cryst. Growth Des.* 14(12) (2014) 6399-6408.

7. Peng CS, Fedeles BI, Singh V, Li D, Amariuta T, Essigmann JM, Tokmakoff A, Two-dimensional IR spectroscopy of the anti-HIV agent KP1212 reveals protonated and neutral tautomers that influence pH-dependent mutagenicity, PNAS, 2015; 112(11): 3229-3234.

8. Urzúa A, Rezende M C, Mascayano C, Vásquez L, Molecules, 2008; 13: 882-891.

9. Anchoori R K, Quirine Kortenhorst MS, Hidalgo M, Sarkar T, Hallur G, Bai R, Van Diest PJ, Hamel E, Khan SR, *J. Med. Chem.* 2008; 51(19): 5953–5957.

10. IDX-184 is a superior HCV direct-acting antiviral drug: a QSAR study, Medicinal Chemistry Research, 2016; 25(5): 1005-1008.

11. Elfiky AA, Elshemey WM, Gawad WA, 2′-Methylguanosine Prodrug (IDX-184), Phosphoramidate Prodrug (Sofosbuvir), Diisobutyryl Prodrug (R7128) Are Better Than Their Parent Nucleotides and Ribavirin in Hepatitis C Virus Inhibition: A Molecular Modeling Study, Journal of Computational and Theoretical Nanoscience, 2015; 12:376–386.

12. Kawakami K, Dynamics of Ribavirin Glass in the Sub-T_g Temperature Region, *J. Phys. Chem. B,* 2011; 115(39): 11375–11381.

13. Vîjan LE, Topală CM, Molecular modeling of ribavirin-DNA interaction, International J. Biology and Biomedical Engineering, 2016; 10: 18-24.

14. Márquez MB, Brandán SA, A structural and vibrational investigation on the antiviral deoxyribonucleoside thymidine agent in gas and aqueous solution phases, International J. of Quantum Chem. 2014; 114(3): 209-221.

15. Brandán SA, Structural, topological, electronic and vibrational properties of the antiviral trifluridine agent. Their comparison with thymidine, Paripex A Indian Journal of Research, 2017; 6(10): 346-360.

16. Romani D, Brandán SA, Spectroscopic and Structural Study of the Antiviral Idoxuridine Agent by Using DFT and SCRF Calculations, IJSRM, International Journal of Science And Research Methodology, 2017; 8(1): 66-86.

17. Romani D, Brandán SA, Investigating the Structural and Vibrational Properties of the Nucleoside Reverse Transcriptase Inhibitor Emtricitabine, IJSRM, International Journal of Science And Research Methodology, 2017; 8(1): 236-277.

18. Iramain MA, Ledesma AE, Romani D, Brandán SA, Structural, electronic, topological and vibrational properties of isomers of thymidine. A study combining spectroscopic data with DFT calculations, IJSRM, International Journal of Science And Research Methodology, 2017; 8(2): 197-238.

19. Topală C M, Temperature effects on the FTIR Spectra of Ribavirin, Rev. Chim. (Bucharest) 2013; 64(2): 132-135.

20. Kumar A, Development and characterization of ribavirin loaded poly (lactide-co-glycolide) nanoparticles by double emulsification method, Jadavpur University Kolkata, India, 2012-2013.

21. Yang H, Liu Y, Huang Y, Tang B, Guo D, Li H, Determination of Ribavirin and Moisture in Pharmaceuticals by Near-Infrared Spectroscopy, Analytical Letters, 2016; 49(13): 2077-2091.

22. Rizwana FB, Muthu S, Prasana JC, Abraham CS, Raja M, Spectroscopic (FT-IR, FT-Raman) investigation, topology (ESP, ELF, LOL) analyses, charge transfer excitation and molecular docking (dengue, HCV) studies on ribavirin, Chemical Data Collections, 2018; 17–18: 236-250.

23. Becke AD, Density functional thermochemistry. III. The role of exact exchange J. Chem. Phys. 1993; 98: 5648-5652.

24. Lee C, Yang W, Parr RG, Development of the Colle-Salvetti correlation-energy formula into a functional of the electron density, Phys. Rev. 1988; B37: 785-789.

25. [Miertus S, Scrocco E, Tomasi J. Electrostatic interaction of a solute with a continuum. Chem. Phys. 1981; 55:117–129.

26. Tomasi J, Persico J. Molecular Interactions in Solution: An Overview of Methods Based on Continous Distributions of the Solvent. Chem. Rev. 1994; 94:2027-2094.

27. Marenich AV, Cramer CJ, Truhlar D.G. Universal solvation model based on solute electron density and a continuum model of the solvent defined by the bulk dielectric constant and atomic surface tensions. J. Phys. Chem. 2009; B113:6378-6396.

28. Ugliengo P, MOLDRAW Program, University of Torino, Dipartimento Chimica IFM, Torino, Italy, 1998.

29. Parr RG, Pearson RG, Absolute hardness: companion parameter to absolute electronegativity, J. Am. Chem. Soc. 1983; 105: 7512-7516.

30. Brédas J-L, Mind the gap!, Materials Horizons, 2014; 1: 17–19.

31. Márquez MJ, Márquez MB, Cataldo PG, Brandán SA, A Comparative Study on the Structural and Vibrational Properties of Two Potential Antimicrobial and Anticancer Cyanopyridine Derivatives, Open Journal of Synthesis Theory and Applications, 2015; 4: 1-19.

32. Cataldo PG, Castillo MV, Brandán SA, Quantum Mechanical Modeling of Fluoromethylated-pyrrol Derivatives a Study on their Reactivities, Structures and Vibrational Properties, J Phys Chem Biophys, 2014; 4(1): 2-9.

33. Romani D, Brandán SA, Márquez MJ, Márquez MB, Structural, topological and vibrational properties of an isothiazole derivatives series with antiviral activities, J. Mol. Struct. 2015; 1100: 279-289.

34. Romani D, Tsuchiya S, Yotsu-Yamashita M, Brandán SA, Spectroscopic and structural investigation on intermediates species structurally associated to the tricyclic bisguanidine compound and to the toxic agent, saxitoxin, J. Mol. Struct. 2016; 1119: 25-38.

35. Romano E, Castillo MV, Pergomet JL, Zinczuk J, Brandán SA, Synthesis, structural and vibrational analysis of (5,7-Dichloro-quinolin-8-yloxy) acetic acid, J. Mol. Struct. 2012; 1018: 149–155.

36. Chain FE, Ladetto MF, Grau A, Catalán CAN, Brandán SA, Structural, electronic, topological and vibrational properties of a series of N-benzylamides derived from Maca (Lepidium meyenii) combining spectroscopic studies with ONION calculations, J. Mol. Struct. 2016; 1105: 403-414.

37. Chain F, Iramain MA, Grau A, Catalán CAN, Brandán SA, Evaluation of the structural, electronic, topological and vibrational properties of N-(3,4-dimethoxybenzyl)-hexadecanamide isolated from Maca (Lepidium meyenii) using different spectroscopic techniques, J. Mol. Struct. 2016; 1119: 25-38.

38. Minteguiaga M, Dellacassa E., Iramain MA, Catalán CAN., Brandán SA, A structural and spectroscopic study on carquejol, a relevant constituent of the medicinal plant Baccharis trimera (Less.) DC. (Asteraceae), J. Mol. Struct. 2017; 1150: 8-20.

39. Iramain MA, Davies L, Brandán SA, Structural and spectroscopic differences among the Potassium 5-hydroxypentanoyltrifluoroborate salt and the furoyl and isonicotinoyl salts, J Mol. Struct. 2019; 1176: 718-728.

40. Issaoui N, Ghalla H, Brandán SA, Bardak F, Flakus HT, Atac A, Oujia B, Experimental FTIR and FTRaman and theoretical studies on the molecular structures of monomer and dimer of 3-thiopheneacrylic acid, J. Mol. Struct. 2017; 1135: 209-221.

41. Minteguiaga M, Dellacassa E, Iramain MA, Catalán CAN, Brandán SA, FT-IR, FT-Raman, UV-Vis, NMR and structural studies of Carquejyl Acetate, a component of the essential oil from *Baccharis trimera* (Less.) DC. (Asteraceae), submitted to J Mol. Struct. 2019; 1177: 499-510. and nucleophilicity, Tetrahedron Letters, 54 (2013) 339-342.

42. Romani D, Brandán SA, Structural and spectroscopic studies of two 1,3-benzothiazole tautomers with potential antimicrobial activity in different media. Prediction of their reactivities, Computational and Theoretical Chemistry, 2015; 1061: 89-99.

43. Kiyooka S, Kaneno D, Fujiyama R, Parr's index to describe both electrophilicity and nucleophilicity, Tetrahedron Letters, 2013; 54: 339-342.

44. Rauhut G, Pulay P, Transferable Scaling Factors for Density Functional Derived Vibrational Force Fields, J. Phys. Chem. 1995; 99: 3093-3100. b) Correction: G. Rauhut, P. Pulay, J. Phys. Chem. 1995; 99: 14572.

45. Sundius T. Scaling of ab-initio force fields by MOLVIB. Vib. Spectrosc. 2002; 29:89-95.

46. Checa MA, Rudyk RA, Chamorro EE, Brandán SA, Chapter 1, Structural and Vibrational Properties of a reverse Inhibitor against the HIV Virus, Dideoxynucleoside Zalcitabine in Gas and Aqueous Solution Phases, pg. 1-26, Edited Collection, Nova Science Publishers, Inc. (2015).

47. Rudyk RA, Ramos ME, Checa MA, Chamorro EE, Brandán SA, Chapter 4, Structural and vibrational properties of 5-trifluoromethyluracil derivative combining DFT and SCRF calculations with SQM methodology, pg. 77-107, Edited Collection, Nova Science Publishers, Inc. (2015).

48. Romani D, Brandán SA, Effect of the side chain on the properties from cidofovir to brincidofovir, an experimental antiviral drug against to *Ebola* virus disease, Arabian J. Chem. (2015). 10.1016/j.arabjc.2015.06.030.

49. Sanmarti B, Maimo Berenguer M, Solsona Rocabert R, Gabriel J, European Patent Application, EP 2 377 862 A1 19.10.2011 Bulletin 2011/42.

50. Prusiner P, Sundaralingam M, The crystal and molevular structures of two polymorphic crystalline forms of virazole(1-β-D-Ribofuranosyl-1,2,4-traizole-3-carboxamide). A new synthetic broad spectrum antiviral agent, Acta Cryst. 1976; B32: 419-426.

51. Nielsen AB, Holder AJ, *Gauss View* 5.0, User's Reference, GAUSSIAN Inc., Pittsburgh, PA, 2008.

52. Gaussian 09, Revision A.02, Frisch, M. J.; Trucks, G. W.; Schlegel, H. B.; Scuseria, G. E.; Robb, M. A.;Cheeseman, J. R.; Scalmani, G.; Barone, V.; Mennucci, B.; Petersson, G. A.; Nakatsuji, H.; Caricato, M.; Li, X.; Hratchian, H. P.; Izmaylov, A. F.; Bloino, J.; Zheng, G.; Sonnenberg, J. L.; Hada, M.; Ehara, M.; Toyota, K.; Fukuda, R.; Hasegawa, J.; Ishida, M.; Nakajima, T.; Honda, Y.; Kitao, O.; Nakai, H.; Vreven, T.; Montgomery, J. A., Jr.; Peralta, J. E.; Ogliaro, F.; Bearpark, M.; Heyd, J. J.; Brothers, E.; Kudin, K. N.; Staroverov, V. N.; Kobayashi, R.; Normand, J.; Raghavachari, K.; Rendell, A.; Burant, J. C.; Iyengar, S. S.; Tomasi, J.; Cossi, M.; Rega, N.; Millam, J. M.; Klene, M.; Knox, J. E.; Cross, J. B.; Bakken, V.; Adamo, C.; Jaramillo, J.; Gomperts, R.; Stratmann, R. E.; Yazyev, O.; Austin, A. J.; Cammi, R.; Pomelli, C.; Ochterski, J. W.; Martin, R. L.; Morokuma, K.; Zakrzewski, V. G.; Voth, G. A.; Salvador, P.; Dannenberg, J. J.; Dapprich, S.; Daniels, A. D.; Farkas, Ö.; Foresman, J. B.; Ortiz, J. V.; Cioslowski, J.; Fox, D. J. Gaussian, Inc., Wallingford CT, 2009.

53. Reed AE, Curtis LA, Weinhold F, Intermolecular interactions from a natural bond orbital, donor-acceptor viewpoint, Chem. Rev. 1988; 88(6): 899-926.

54. Glendening ED, Badenhoop JK, Reed AD, Carpenter J E, Weinhold F, NBO 3.1; Theoretical Chemistry Institute, University of Wisconsin; Madison, WI, 1996.

55. Bader RFW, Atoms in Molecules, A Quantum Theory, Oxford University Press, Oxford, 1990, ISBN: 0198558651.

56. Biegler-Köning F, Schönbohm J, Bayles D, AIM2000; A Program to Analyze and Visualize Atoms in Molecules, J. Comput. Chem. 2001; 22: 545-559.

57. Besler BH, Merz KM Jr, Kollman PA, Atomic charges derived from demiempirical methods, J. Comp. Chem. 1990; 11: 431-439.

58. Romano E, Ladetto F, Brandán SA, Structural and Vibrational studies of the potential anticancer agent, 5-difluoromethyl-1,3,4-thiadiazole-2-amino by DFT calculations, Comput. Theoret. Chem. 2013; 1011: 57-64.

59. Romano E, Soria NAJ, Rudyk R, Brandán SA, Structural and Vibrational Properties of a 1,3,4-Oxadiazole derivative with diverse biological activities, J. Asia Spectrosc. 2013; 17: 1-28.

60. Romano E, Soria NAJ, Rudyk R, Brandán SA, Theoretical Study of the infrared spectrum of 5-phenyl-1,3,4-oxadiazole-2-thiol by using DFT calculations, J. Molec. Simul. 2012; 38(7): 561-566.

61. Romano E, Soria NAJ, Rudyk R, Brandán SA, Theoretical structural and vibrational study of a potential bioactive agent: the (5-pyridin-4-yl)-1,3,4-Oxadiazole-2-thiol compound, Asian Materials Science Letters, 2013; 2: 1-14.

62. Márquez MJ, Márquez MB, Ladetto MF, Brandán SA, A structural and vibrational investigation on a material for sodium-ion batteries, the NASICON-type $Na_3V_2(PO_4)_3$ compound based on *Ab-Initio* calculations, ChemXpress, 2015; 8(2): 57-73.

63. Bushmarinov IS, Lyssenko KA, Yu Antipin M, Russian Chem. Rev. 2009; 78(4): 283-302.